



1 **Impact of Solar Geoengineering on Wildfires in the 21st Century in**
2 **CESM2/WACCM6**

3
4 **Wenfu Tang¹, Simone Tilmes¹, David M. Lawrence², Fang Li³, Cenlin He⁴, Louisa K.**
5 **Emmons¹, Rebecca R. Buchholz¹, Lili Xia⁵**

6
7 ¹Atmospheric Chemistry Observations & Modeling Laboratory, National Center for Atmospheric
8 Research, Boulder, CO, USA

9 ²Climate and Global Dynamics Laboratory, National Center for Atmospheric Research, Boulder,
10 CO, USA

11 ³International Center for Climate and Environment Sciences, Institute of Atmospheric Physics,
12 Chinese Academy of Sciences, Beijing, China

13 ⁴Research Applications Laboratory, National Center for Atmospheric Research, Boulder, CO,
14 USA

15 ⁵Department of Environmental Sciences, Rutgers University, New Brunswick, NJ, USA

16

17

18 Correspondence: Wenfu Tang (wenfut@ucar.edu)

19

20

21

Abstract

22 We quantify future changes of wildfire burned area and carbon emissions in the 21st
23 century under four Shared Socioeconomic Pathways (SSPs) scenarios and two SSP5-8.5-based
24 solar geoengineering scenarios with a target surface temperature defined by SSP2-4.5: solar
25 irradiance reduction (G6solar) and stratospheric sulfate aerosol injections (G6sulfur), and explore
26 the mechanisms that drive solar geoengineering impacts on fires. This study is based on fully
27 coupled climate-chemistry simulations with simulated occurrence of fires (area burnt and carbon
28 emissions) using the Whole Atmosphere Community Climate Model Version 6 (WACCM6) as
29 the atmospheric component of the Community Earth System Model Version 2 (CESM2). Globally,
30 total wildfire burned area is projected to increase over the 21st century under scenarios without
31 geoengineering and decrease under the two geoengineering scenarios. By the end of the century,
32 the two geoengineering scenarios have lower burned area and fire carbon emissions than not only
33 their base-climate scenario SSP5-8.5 but also the targeted-climate scenario SSP2-4.5.

34 Geoengineering reduces wildfire occurrence through decreasing surface temperature and
35 wind speed and increasing relative humidity and soil water, with the exception of boreal regions
36 where geoengineering increases the occurrence of wildfires due to a decrease in relative humidity
37 and soil water compared to present day. This leads to a global reduction in burned area and fire
38 carbon emissions by the end of the century. However, geoengineering also yields reductions in
39 precipitation compared to a warming climate, which offsets some of the fire reduction. Overall,
40 the impacts of the different driving factors are larger on burned area than fire carbon emissions. In
41 general, the stratospheric sulfate aerosol approach has a stronger fire-reducing effect than the solar
42 irradiance reduction approach.

43



44 1. Introduction

45 Fire is an important component of the Earth system. It directly impacts climate in two main
46 ways. First, the burning of biomass is one of the major sources of radiatively and/or chemically
47 active trace gases and aerosols in the atmosphere (Andreae and Merlet, 2001; Li et al. 2022).
48 Second, fires pose alterations to terrestrial ecosystem states and functioning such as changing
49 vegetation distribution and structure, disturbing the carbon cycle and water cycle, and changing
50 surface albedo (Bowman et al., 2009; Li and Lawrence, 2017; Liu et al., 2019; Lasslop et al. 2020).
51 In addition to the impact on climate, fires also have significant impacts on air quality and weather
52 across spatial scales (e.g., Bowman et al., 2009, Tang et al., 2022). For example, fires degrade air
53 quality and human health as many of the emitted gases and aerosols from fires are primary
54 pollutants or precursors to secondary chemically-produced pollutants (Wiedinmyer et al., 2006;
55 van der Werf et al., 2006). Fires also alter regional dynamics and weather through changing surface
56 heat and water vapor fluxes, convection, clouds, and precipitation (e.g., Bowman et al., 2009; Coen
57 et al., 2013, Zhang et al., 2022).

58 Fire is regulated by various factors, including weather and climate conditions (e.g., soil
59 moisture, temperature, precipitation, and wind speed), vegetation composition and structure, and
60 human activities (e.g., land use and land cover change, human ignition and suppression) (e.g., Li
61 et al., 2013; Chen et al., 2017; Knorr et al., 2016a, 2016b; Li et al., 2018; Pechony and Shindell,
62 2010; van der Werf et al., 2008). These factors also interact with each other in the Earth system
63 (e.g., Walker et al., 2020; Loehman, 2020). For example, climate can alter vegetation composition
64 and structure, and vegetation can also impact climate and weather through evapotranspiration. Due
65 to the complex interactions and feedbacks among these factors and fires, quantifying and
66 projecting the trend of fires is challenging and is subject to large uncertainties. Despite challenges
67 and uncertainties, previous studies have generally suggested that in the future global fire risk will
68 increase, though with significant regional differences (e.g., Abatzoglou et al., 2019; Bowman et
69 al., 2020; Di Virgilio et al., 2019; Flannigan et al., 2009, 2013; Ford et al., 2018; Huang et al.,
70 2015; Li et al., 2020; Liu et al. 2010; Luo et al., 2013; Pechony and Shindell, 2010; Veira et al.,
71 2016). The growing importance combined with large uncertainties of fires has posed an urge to
72 understand and quantify future fire trends in the context of climate change. It has been suggested
73 that future climate mitigation should consider the impact of fires (Shiogama et al., 2020; Ward et
74 al., 2012).

75 The Shared Socioeconomic Pathways (SSPs) were established to facilitate the integrated
76 analysis of future climate impacts, vulnerabilities, adaptation, and mitigation (Riahi et al., 2017).
77 These SSP scenarios utilized in Phase 6 of the Coupled Model Intercomparison Project (CMIP6)
78 were generated with integrated assessment models, based on five narratives describing alternative
79 socio-economic developments, including sustainable development (SSP1), middle-of-the-road
80 development (SSP2), regional rivalry (SSP3), inequality (SSP4), and fossil-fueled development
81 (SSP5). Different scenarios have different energy, land use, and emissions implications.
82 Corresponding global population projections consistent with each of the SSPs have also been
83 established (Jones and O'Neill, 2016).

84 Solar geoengineering, also known as solar radiation modification (SRM) or more generally as
85 climate intervention, has been researched as a potential option to offset some of the radiative
86 effects of increasing anthropogenic greenhouse gases in the future through solar radiation



87 modification (e.g., Kravitz et al., 2015; Tilmes et al., 2009, 2020). One proposed approach is to
88 inject the precursor of sulfate aerosols (sulfur dioxide; SO_2) to the stratosphere that can reflect
89 incoming solar radiation. To understand the impacts of sulfate aerosols compared to direct solar
90 irradiance reduction, both experiments have been performed in parallel (e.g., Xia et al., 2016,
91 Visionsi et al., 2021a). Previous studies have analyzed the impact of geoengineering on climate
92 outcomes (e.g., Tilmes et al., 2013, 2020; Visionsi et al., 2021a). While global surface temperature
93 targets could be reached, SRM approaches tend to overcompensate the hydrological cycle, with
94 potential consequences to other impacts on climate and the Earth system (Robock, 2020). Since
95 fire is a key component of the Earth system and the drivers of fires are directly or indirectly
96 changed by solar geoengineering, the impacts of solar geoengineering on fires should also be
97 considered when designing and assessing solar geoengineering approaches.

98 In this paper, we use a fully coupled Earth system model CESM2 with WACCM6 as the
99 atmospheric component. CESM2 (WACCM6) is coupled to the Community Land Model (CLM)
100 that includes a prognostic fire scheme, which interacts with various land and atmospheric
101 processes. WACCM6 is currently not using biomass burning emissions derived from the land
102 model. However, while this feedback is missing, the fire model still responds to changes in the
103 land and atmosphere and is therefore suited to investigate how fires change in the 21st century.
104 We analyze the future trends of burned area and fire carbon emissions under the two
105 geoengineering scenarios and SSP scenarios, and then analyze how the two solar geoengineering
106 approaches impact fire activity. This paper is organized as follows: Section 2 describes the model
107 simulations; Section 3 presents the future trends of burned area and fire carbon emissions under
108 SSP scenarios and geoengineering scenarios. Section 4 discusses how geoengineering impacts fire,
109 and Section 5 concludes the study.

110

111 **2. Model descriptions and simulations**

112 **2.1 CESM2 (WACCM6)**

113 CESM2 (WACCM6) is a community model that has components of ocean, atmosphere, land,
114 sea-ice, land-ice, river, and wave models. These components are coupled in CESM2 by exchanging
115 states and fluxes via a coupler (Danabasoglu et al., 2019). The Community Land Model Version
116 5 (CLM5) is the land component of CESM2 (Lawrence et al., 2019). CLM uses prescribed
117 temporal land use and land cover change (LULCC), which consists of an annual time series of the
118 spatial distribution of the naturally vegetated and cropland units of each grid cell, combined with
119 the distribution of plant functional types (PFTs) and crop functional types (CFTs) existing in those
120 land units (Lawrence et al., 2019). The interactive fire scheme in the CLM5 is a key component of
121 this study and is described in more detail in Section 2.2. WACCM6 is a high-top atmospheric
122 model with 70 vertical levels and model top at ~ 140 km, therefore it has reasonable representation
123 of the stratosphere. WACCM6 also includes comprehensive chemistry and aerosol mechanisms
124 (Gettelman et al., 2019; Emmons et al., 2020, Tilmes et al., 2019).

125 **2.2 Description and evaluation of fire scheme in CESM2/CLM5**



126 The fire scheme in CESM2/CLM5 accounts for four types of fires: agricultural fires in
127 cropland, deforestation fires in the tropical closed forests, peat fires, and non-peat fires outside
128 cropland and tropical closed forests (Li et al., 2012, 2013). Agricultural fire is accounted for in
129 these simulations but is not included in the analysis, since we focus on wildfires here. In the fire
130 scheme, burned area is affected by climate and weather conditions, vegetation composition and
131 structure, and human activities. Climate and weather conditions (e.g., temperature, precipitation,
132 wind, humidity, and soil moisture) impact natural and human ignition and fire spread through fuel
133 availability and fuel combustibility. Human activities impact deforestation fires via deforestation
134 rates that are applied from the Land Use Harmonization dataset (LUH2, Hurtt et al., 2020) that is
135 used in these experiments. Human impacts on non-deforestation and non-peat fires include both
136 ignition and suppression and are parameterized as functions of both population density and Gross
137 Domestic Product (GDP). In our setup, the global population scenarios corresponding to SSP
138 scenarios (Jones and O'Neill, 2016) are used while regionally-explicit GDP was held constant for
139 all WACCM6 simulations analyzed in this study. Fire-induced changes (including biomass and
140 peat burning, vegetation mortality, adjustment of the carbon and nitrogen (C/N) pools, carbon
141 emissions, changes in vegetation structure and functioning as well as surface water and energy
142 fluxes) are then simulated based on the calculated burned area (Li et al., 2012, 2013). These fire-
143 induced surface property changes in the land model further alter atmospheric states (i.e.,
144 temperature and water vapor) in the coupled model. Although the burned area and fire carbon
145 emissions are simulated in CLM5, our CESM2/(WACCM6) simulations use prescribed fire
146 emissions based on the CMIP6 projected inventories for trace gases and aerosols (Riahi et al., 2017)
147 for different SSPs and geoengineering scenarios. Full coupling of simulated fire aerosol emissions
148 is an area of ongoing development and analysis with the CESM project.

149 The fire scheme in CESM has been validated and evaluated in both uncoupled and coupled
150 versions (Li et al., 2012, 2013, 2017, 2018; Li and Lawrence 2017) and compared with other fire
151 models within the Fire Modeling Intercomparison Project (FireMIP) (Li et al., 2019). Evaluation
152 results have shown that the fire scheme can reasonably reproduce the observed amount, spatial
153 pattern, seasonality, and interannual variability of global fires, and fire-population relationship
154 under present-day climate, and has a similar historical long-term trend to the multi-source merged
155 historical reconstructions used as input data for CMIP6 (Li et al. 2018, Li et al. 2019). Although
156 the model underestimates the climate impacts on fires in boreal North America, it still performs
157 better than many other fire models (Yue et al., 2016). Here we briefly evaluate the fire carbon
158 emissions from the CESM2 (WACCM6) simulations with two satellite-based fire emission
159 inventories, namely FINNv2.5 (Fire INventory from NCAR Version 2.5; Wiedinmyer et al., 2022)
160 and GFED4.1s (Global Fire Emissions Database, Version 4.1s; Randerson et al., 2018). The annual
161 total emissions and global distributions of WACCM simulations agree well with those from
162 FINNv2.5 and GFED4.1s (Figures S1 and S2). The annual total fire carbon emissions during 2015-
163 2019 estimated from the WACCM simulations (2.5 PgC/yr) fall into the range of GFED4.1s (2.0
164 PgC/yr) and FINNv2.5 (3.8 PgC/yr).

165 **2.3 SSPs and geoengineering scenarios**

166 The Scenario Model Intercomparison Project (ScenarioMIP) based on SSPs is the primary
167 activity within CMIP6 that provides multi-model climate projections based on alternative
168 scenarios (O'Neill et al., 2016). These climate projections are driven by SSP scenarios and are
169 related to the Representative Concentration Pathways (RCPs) as described below. The Land Use



170 Model Intercomparison Project (LUMIP) also provides LULCC data for SSPs (Lawrence et al.,
171 2016, Hurtt et al., 2020). In this study, the SSP1-2.6, SSP2-4.5, SSP3-7.0, and SSP5-8.5 scenarios
172 (O'Neill et al., 2016) are shown. (1) SSP1-2.6 (sustainable development) is the low end of the
173 range of future forcing pathways in SSP and updates the RCP2.6 scenario. SSP1 includes
174 substantial land use change, particularly with increasing global forest cover. (2) SSP2-4.5 is a
175 scenario that represents the middle part of the range of future forcing pathways and updates the
176 RCP4.5 scenario. Land use and aerosol changes in SSP2 (middle-of-the-road development) are
177 not extreme relative to other SSPs. (3) SSP3-7.0 is a scenario with both substantial land use
178 changes (particularly decreased global forest cover) and high near-term climate forcings emissions,
179 particularly sulfur dioxide (SO₂). (4) SSP5-8.5 is the unmitigated baseline scenario, representing
180 the high end of the range of future pathways, and updates the RCP8.5 scenario. There is relatively
181 little land-use change in the 21st century in this scenario which leads to slow decline in the rate of
182 deforestation (O'Neill et al., 2017).

183 The Geoengineering MIP Phase 6 (GeoMIP6) proposed experiments for future projection with
184 geoengineering measures implemented based on ScenarioMIP. In this study we also analyze the
185 response of wildfires under two of the geoengineering experiments – G6Sulfur and G6Solar
186 (Kravitz et al., 2015). Both of these geoengineering scenarios aim to reduce forcing from
187 ScenarioMIP Tier 1 high forcing scenario (SSP5-8.5) to the medium forcing scenario (SSP2-4.5),
188 going from 8.5 to 4.5 Wm⁻² in 2100.

189 G6Sulfur reduces forcing with stratospheric sulfate aerosols. In G6Sulfur experiment, SO₂, the
190 precursor of stratospheric sulfate aerosol has been continuously injected into the model at 25 km
191 altitude at the Equator with the goal of reducing the magnitude of the net anthropogenic radiative
192 forcing and reaching surface temperatures at SSP2-4.5 levels.

193 G6Solar uses the same setup as G6sulfur, but uses solar irradiance reduction to reduce the
194 magnitude of the net anthropogenic radiative forcing. The reduction of the solar constant in
195 G6Solar and the injected SO₂ in G6Sulfur is determined by a feedback algorithm described in
196 Kravitz et al. (2017) and used in Tilmes et al. (2018, 2020).

197 **2.4 Simulations**

198 In this study we analyze results from fully coupled WACCM6 simulations for future projection
199 under the aforementioned scenarios from GeoMIP and ScenarioMIP. The continuous long-term
200 (2015 to 2100) simulations used in this study provide a continuous picture of future fire changes
201 and allow us to investigate when and how major changes in the fire trends occur. The horizontal
202 resolution for land and atmosphere is 1.25° × 0.9° (longitude × latitude). Multiple simulations (2~5
203 members) are conducted for each scenario except for the SSP1-2.6 and SSP3-7.0 scenarios (see
204 Table S1). WACCM6 historical simulations serve as initial conditions for the future scenarios.
205 Future climate under these simulations has been analyzed in Meehl et al. (2020) and Jones et al.
206 (2020).

207 **3 Future trends of fires**

208 **3.1 Future trends of burned area and fire carbon emissions under the SSP scenarios**



209 The global total wildfire burned area in these simulations is projected to increase under all
210 the SSP scenarios (Figure 1a). The largest increases in the global burned area are seen in the SSP5-
211 8.5 scenarios (~20%) and SSP3-7.0 (~10%). The changes in the other scenarios are relatively small
212 (Table S2). In terms of the spatial distribution, the 40°N–70°N latitude is the only latitude band in
213 which the burned area consistently increases under all the SSP scenarios (Figure 1b). In the 10°S–
214 5°N latitude band (tropical region), the burned area consistently decreases under all scenarios to a
215 diverse extent. A more detailed discussion on future trends of fire activity under the SSP scenarios
216 are provided in the Supplement.

217 3.2 Future trends of burned area and fire carbon emissions with geoengineering

218 The two geoengineering scenarios (G6Sulfur and G6Solar) are based on SSP5-8.5 and
219 targeted SSP2-4.5. As G6Sulfur reduces the forcing through stratospheric sulfate aerosols while
220 G6Solar directly decreases total incoming solar irradiance, the difference between the two provides
221 insight on the other impacts of sulfate aerosols on fires besides the forcing change. Even though
222 fire carbon emissions are largely driven by burned area, they are also impacted by fuel availability
223 and combustion completeness. Therefore, the fire carbon emissions and burned area generally
224 show trends consistent with burned area, with some notable differences. Both burned area and fire
225 carbon emissions under the two geoengineering scenarios are lower than those under SSP5-8.5
226 (Figures 2a and 2c). Lower fire activity in these geoengineering scenarios than SSP5-8.5 is
227 expected due to reduced surface warming towards SSP2-4.5 target climate conditions. However,
228 we found that by the end of the century, the two geoengineering scenarios have lower burned area
229 and fire carbon emissions than not only their base-forcing scenario SSP5-8.5 but also the targeted-
230 forcing scenario SSP2-4.5 (Figures 2a and 2c). The change of the two geoengineering scenarios
231 compared to SSP2-4.5 by the end of the century is small in burned area (-2% – -12%) but relatively
232 large in fire carbon emissions (-18% – -23%). However, when compared to SSP5-8.5, the
233 reduction of the two geoengineering scenarios in burned area (-18% – -26%) is similar to that in
234 fire carbon emissions (-20% – -26%). This implies that the difference in fire carbon emissions
235 between the two geoengineering scenarios and SSP2-4.5 are less driven by burned area and that
236 fuel availability plays a more important role in this comparison, while for the difference to SSP5-
237 8.5, changes in burned area plays more of a role in emission differences. The two geoengineering
238 approaches (G6solar and G6sulfur) generally lead to reduced fire activity compared to SSP5-8.5
239 in most regions in 2091-2100, except for Northern Hemisphere Africa and Equatorial Asia
240 (Figures S3 and S4). When comparing the period 2091-2100 to the period 2021-2030, the largest
241 decrease in global total wildfire burned area is seen in the G6sulfur scenario among all the
242 scenarios in this study (~ -11%; see Table S2).

243 In the 40°N–70°N latitude band, the burned area consistently increases under not only all
244 the SSP scenarios but also the two geoengineering scenarios when comparing the period 2091-
245 2100 to the period 2021-2030 (Figure 2b). However, the increase in burned area is lower in the
246 two geoengineering scenarios compared to SSP5-8.5 and is similar to the SSP2-45 scenario. In the
247 -20°S–0° latitude band, the reduction in burned area is larger under G6sulfur than that under
248 G6Solar (Figure 2a). Generally, G6sulfur has a stronger fire-reducing effect than G6solar, with
249 exceptions such as over Europe. We also found notable differences between the two
250 geoengineering methods for some specific regions, implying that the geoengineering method
251 chosen could be inequitable for some countries. For example, G6Solar is the better choice for



252 producing less burned area in Europe, while over Southern Hemisphere Africa, G6Sulfur is better
253 than G6Solar (see Figure S4).

254 **4 Mechanism of geoengineering impacting fires**

255 The two SSP5-8.5-based geoengineering scenarios successfully reduce the radiative
256 forcing from 8.5 Wm^{-2} (as in SSP5-8.5) to 4.5 Wm^{-2} (as in SSP2-4.5) in 2100 and global surface
257 temperatures between SSP2-4.5 and the two geoengineering scenarios are nearly the same.
258 However, both geoengineering scenarios produce less fire than SSP2-4.5 by 2100 (Figures 2 and
259 3). There are different processes involved in the cooling in G6Sulfur (due to the stratospheric
260 sulfate aerosols) and the cooling in G6Solar (due to directly reduced insolation) (Visioni et al.,
261 2021a). Because of the difference in the resulting climate response, these two geoengineering
262 approaches impact fires differently, even though they are designed to achieve the same forcing
263 level by 2100. Previous studies indicate that stratospheric heating caused by aerosols can impact
264 precipitation and temperature at the surface through alterations to stratospheric dynamics (Jiang et
265 al., 2019; Simpson et al., 2019; Richter et al., 2017; Visioni et al., 2020). Last but not least, the
266 two geoengineering approaches also result in different outcomes for other quantities important for
267 fires. For example, enhanced stratospheric aerosol burden results in changes in direct to diffuse
268 light which promotes plant growth (e.g., Xia et al., 2017; Xu et al., 2020). On the other hand, it
269 can reduce in the hydrological cycle and regional precipitation changes due to the aerosol heating
270 effects in the lower tropical stratosphere (e.g., Tilmes et al., 2013, Simpson et al., 2019).

271 Here we analyze the key variables in the Earth system that are involved in the processes
272 from the reduced insolation on the top of the atmosphere and sulfate aerosols in the stratosphere
273 to fires at the surface. Note that hereafter for a scenario with multiple ensemble members, only the
274 ensemble mean is analyzed and shown. The key variables shown in this section are selected via
275 comparing the key variables that determine fire activity in the fire scheme in CESM2/CLM5 with
276 the key climate variables that are impacted by geoengineering approaches. The analyses are
277 conducted for 14 individual fire regions following Giglio et al. (2010), namely Boreal North
278 America, Temperate North America, Central America, Northern Hemisphere South America,
279 Southern Hemisphere South America, Europe, Middle East, Northern Hemisphere Africa,
280 Southern Hemisphere Africa, Boreal Asia, Central Asia, Southeast Asia, Equatorial Asia, and
281 Australia and New Zealand (Figure S3).

282 **4.1 Surface temperature**

283 Even though the mean surface temperature (TS) for the whole globe and the land are similar
284 under the two geoengineering scenarios and SSP2-4.5 (Figure 4), regional differences exist
285 (Figures 5). For example, over Equatorial Asia, the annual surface mean temperatures in the two
286 geoengineering scenarios are consistently lower than that in SSP2-4.5 by $\sim 0.3\text{K}$ during 2091-2100
287 (Figure S6). The spatial distribution of burned area difference and fire carbon emission difference
288 between G6Solar/G6Sulfur and SSP5-8.5 (Figure 3) are not always co-located with their spatial
289 distribution of surface temperature difference (Figure 5). To understand to what extent the surface
290 temperature drives fire activity change, we calculate correlations of surface temperature change
291 and burned area/fire carbon emission change for individual fire regions under SSP2-4.5, G6Solar,
292 and G6Sulfur. Surface temperature change (ΔTS) for a given region is calculated based on the
293 individual model grids within the region and annual values between 2091-2100. It is defined as



294 the difference between the analyzed scenario (i.e., G6Solar, G6Sulfur, and SSP2-4.5) and the
295 reference scenario (i.e., SSP5-8.5). Burned area change (ΔBA) and fire carbon emission change
296 (ΔC_{emis}) are defined in the same way. The correlations calculated here account for spatial
297 variability within the region and interannual variability during 2091-2100.

298 Overall, surface temperature plays a more important role in the decrease of fire activity in
299 the two geoengineering scenarios compared to that in SSP2-4.5 relative to SSP5-8.5 (Figure 6).
300 This is expected because the only difference between the two geoengineering scenarios and SSP5-
301 8.5 is the specific application of climate intervention; whereas the differences between SSP2-4.5
302 and SSP5-8.5 involves several other differences including population growth and LULCC. For
303 G6Solar and G6Sulfur, the strongest impact of surface temperature change on burned area occurs
304 over Southern Hemisphere South America (correlation=0.42 for G6Solar and 0.45 for G6Sulfur),
305 followed by Southern Hemisphere Africa, Temperate North America, and Europe. The impact of
306 surface temperature change over boreal regions (Boreal North America and Boreal Asia) are
307 relatively small. This suggests that the changes in area burnt in these regions are not predominantly
308 driven by the surface temperature changes, but by other factors. For G6Solar and G6Sulfur, the
309 impact of surface temperature on burned area is generally larger than its impact on fire carbon
310 emissions. This is expected as fire carbon emissions in CESM2/WACCM6 are determined by
311 burned area together with vegetation characteristics (carbon density and combustion completeness;
312 Li et al., 2012), which introduces more uncertainties. The only exception occurs over the Northern
313 Hemisphere South America where surface temperature plays a more important role in fire carbon
314 emissions than burned area for not only G6Solar (correlation is 0.37 versus 0.29) and G6Sulfur
315 (correlation is 0.37 versus 0.24) but also SSP2-4.5 (correlation is 0.40 versus 0.23). Over Northern
316 Hemisphere South America, the correlations between ΔTS and $\Delta BA/\Delta C_{emis}$ are also close under
317 the three scenarios. Since combustion completeness is a fixed parameter, this difference points to
318 the possibility that the reduced surface temperature has a larger impact on carbon density over
319 Northern Hemisphere South America than over other regions.

320 Overall, we find that the surface temperature change introduced by the two geoengineering
321 approaches (solar irradiance reduction and stratospheric sulfate aerosols) by the end of the century
322 impacts burned area and fire carbon emissions, e.g., the introduced cooling results in smaller fire
323 activity. The degree of impact varies dramatically across different regions. The impact of surface
324 temperature in G6Solar and G6Sulfur are overall close. However, surface temperature alone does
325 not account for all the changes in fire activity.

326 **4.2 Precipitation**

327 Precipitation change is also an important consequence of climate change and
328 geoengineering (Figure 4). Global precipitation is expected to increase under climate change as
329 higher tropospheric temperature leads to more moisture in the air. Previous studies found that
330 geoengineering could eliminate these increases in precipitation and can even reduce global mean
331 or regional precipitation relative to the target scenario, depending on the geoengineering approach
332 (Tilmes et al., 2013, Simpson et al., 2019, Visioni et al., 2021a). The spatial distribution of
333 precipitation changes under G6Solar and G6Sulfur relative to SSP5-8.5 are similar (Figure 5). The
334 trend of precipitation varies dramatically across regions (Figure S8). Precipitation is also important
335 for fires. Precipitation itself could have either a positive or a negative impact on future fires
336 because precipitation can impact both fuel combustibility and fuel availability, which impact fire



337 in opposite directions. In addition, precipitation changes can also lead to changes in relative
338 humidity and soil water content, which are important factors for fires. Here we apply the same
339 analyses for precipitation change (Δ Precip) as in Section 4.1 for surface temperature change (Δ TS).

340 The reduction in precipitation by geoengineering has the opposite impact on fire as the
341 reduction in surface temperature by geoengineering, as shown by the negative correlations of
342 Δ Precip and Δ BA/ Δ Cemis (Figure 6). The correlations are consistently negative across all the
343 scenarios (G6Solar, G6Sulfur, and SSP2-4.5) and almost all regions. The largest impact of
344 precipitation change occurs over Equatorial Asia for all three scenarios (correlation is -0.45–-0.42
345 for Δ BA and -0.43–-0.33 for Δ Cemis), which is aligned with the strong precipitation change over
346 the region (Figures 5). Over the Middle East, precipitation change has a relatively large impact on
347 burned area and fire carbon emissions under G6Solar as well as SSP2-4.5, however the impact is
348 small under G6Sulfur. We note that unlike the impact of Δ TS, the impact Δ Precip is relatively
349 large over boreal regions. We conduct a sensitivity test of 1-year lag correlation to understand the
350 impact of previous year precipitation change on fire activity (for example calculating correlation
351 of Δ Precip for 2091 and Δ BA/ Δ Cemis for 2092). We found that this correlation is still significant
352 for most regions, though it is generally lower. Overall precipitation change is inversely related to
353 burned area change and fire carbon emission change. Therefore, for these regions where
354 precipitation is reduced compared to SSP5-8.5 as a consequence of geoengineering such as
355 Equatorial Asia, the reduction in burned area and fire carbon emissions due to reduced surface
356 temperature are offset to some extent.

357 4.3 Humidity

358 Humidity is also impacted by geoengineering. The future trends of specific humidity (g/kg)
359 and relative humidity (%) are opposite as specific humidity is projected to increase while relative
360 humidity is projected to decrease compared to SSP5-8.5 (Figure 4). Their spatial distribution and
361 inter-scenario differences are also divergent (Figures 4 and 5). This is due to the fact that relative
362 humidity is driven by not only the actual moisture content but also the temperature. The same
363 amount of water vapor results in a higher relative humidity in colder air than in warm air. Therefore
364 a reduction in relative humidity in a warming climate indicates that the relative amount of water
365 vapor has not increased proportional to the warming. Relative humidity is a driving variable in the
366 CLM5 fire module in multiple places (e.g., lower relative humidity leads to higher fuel
367 combustibility and larger fire spread). Here we focus our analysis on the relative humidity change
368 at 2-meter (Δ RH) as relative humidity is directly used in the CLM5 fire module. Changes in
369 relative humidity show different spatial distribution between the G6solar minus SSP5-8.5 and
370 G6sulfur minus SSP5-8.5 (Figure 5), even though their global average values are close (Figure 4).
371 Since 2-meter relative humidity is strongly driven by evapotranspiration, the difference between
372 G6sulfur and G6Solar points to the possibility that stratospheric sulfate aerosols lead to more
373 scattered light and hence enhanced plant growth than the solar case, which results in more
374 evapotranspiration.

375 The relative humidity change (Δ RH) is negatively correlated to Δ BA/ Δ Cemis across all
376 scenarios and regions (Figure 6). Therefore, the higher relative humidity in G6Solar, G6Sulfur,
377 and SSP2-4.5 than SSP5-8.5 (Figure 4) leads to less fire activity globally. Overall, the relative
378 humidity change is more strongly correlated to Δ BA/ Δ Cemis, indicating that relative humidity



379 change is a more important driver of fire activity change under geoengineering than surface
380 temperature or precipitation.

381 4.4 Wind speed

382 Wind speed is also an important driving factor in fire spread and is also indirectly impacted
383 by geoengineering (Figure 4). In CLM5, wind speed is used in the calculation of fire spread and
384 hence burned area. Wind speed mainly has an indirect impact on fire carbon emissions through
385 burned area. Here we analyze 10-meter wind speed (U10). By the end of the century, SSP2-4.5
386 has slightly higher U10 than SSP5-8.5, G6Solar has similar U10 as SSP5-8.5, while G6Sulfur has
387 slightly lower U10 than SSP5-8.5 over land (Figure 4). However, the regional difference can be
388 relatively large (Figures 5). G6sulfur and G6solar have significantly different U10 over Southern
389 Hemisphere ocean (Figures 5). However, the difference in U10 between G6solar and G6sulfur
390 over land is relatively small with exceptions such as over Australia and Northern Hemisphere
391 Africa where G6sulfur has lower U10.

392 Wind speed change has consistently positive correlations with changes in burned area and
393 fire carbon emissions under the two geoengineering scenarios across all analyzed regions (which
394 is not the case for SSP2-4.5, where $\Delta U10$ is negatively correlated ΔBA or ΔC_{emis} over most
395 regions). This indicates that the reduction in wind speed as a byproduct of geoengineering (Figure
396 4) leads to less fire activity globally. The wind speed reduction is relatively large over South
397 Hemisphere Africa (Figure 5), and the correlations are also high, indicating the wind speed
398 reduction is partially responsible for the reduction in fire activity over South Hemisphere Africa.

399 4.5 Soil water content

400 Soil water content is a key driver of fire activity as it impacts fuel combustibility and fire
401 spread. Soil water content is indirectly impacted by the geoengineering approaches through the
402 hydrological cycle. The precipitation changes as a result of geoengineering compared to SSP5-8.5
403 strongly impacts the soil water content, and the soil water content further drives the relative
404 humidity near the surface through evapotranspiration. We see a much smaller reduction in soil
405 water content in the geoengineering runs compared to SSP2-4.5. Therefore, the future trends of soil
406 water content (here we use the model variable SOILWATER_10CM, i.e., the soil water content in
407 the top 10 cm (kg/m^2) to evaluate soil moisture) are close to the future trends of relative humidity
408 (Figure 4) globally. However, in the last decade of the century, difference in soil water content
409 among the scenarios is larger than the difference in relative humidity among the scenarios (the
410 difference of the 3 scenarios from SSP5-8.5 are $\sim 1\text{--}2\%$ for relative humidity and $\sim 4\text{--}7\%$ for
411 SOILWATER_10CM). Here we include analyses of soil water content not only because it is a
412 very important driver of fire activity but also because the spatial distributions of soil water change
413 ($\Delta \text{SOILWATER}$) can be different than relative humidity change in some regions (Figures 5).
414 Overall, similar to precipitation and relative humidity, soil water content change is negatively
415 related to burned area and fire carbon emissions with different spatial distributions (Figure 6). For
416 example, over the boreal regions and Europe, the impact of $\Delta \text{SOILWATER}$ is smaller than the
417 impact of ΔRH , while over Central Asia it is larger.

418 4.6 Others



419 There are other relevant variables that are not analyze in detail here. For example, the
420 reduction in the downwelling solar flux at the surface ($\Delta FSDS$) is a direct consequence of
421 geoengineering (solar irradiance reduction and stratospheric sulfate aerosols). In addition, water
422 vapor content and cloud change as a consequence of geoengineering also impact downwelling
423 solar flux at the surface. We include the analyses of downwelling solar flux in the supplement
424 (Figures S9-S10) as the downwelling solar flux at the surface does not directly determine burned
425 area and fire carbon emissions in the model. The downwelling solar flux at the surface is positively
426 related to burned area and fire carbon emissions. Therefore, the lower downwelling solar flux at
427 the surface than SSP5-8.5 as a result of the geoengineering approaches leads to less fires globally
428 while the higher downwelling solar flux at the surface under SSP2-4.5 than SSP5-8.5 tends to
429 increase fire activity and can offset the overall reduction fires in SSP2-4.5 than SSP5-8.5 to some
430 degree. As another example, vegetation carbon can also impact the total fire carbon emissions and
431 are also impacted by fire activity. However, we do not further analyze the impact of fuel load
432 because geoengineering approaches do not seem to change global total fuel load significantly. The
433 future trend of total vegetation carbon under G6Solar and G6Sulfur are very close to SSP5-8.5,
434 and the three of them are different from SSP2-4.5 as total vegetation carbon is largely driven by
435 CO_2 (Figure 4).

436 4.7 G6Sulfur versus G6Solar

437 Comparisons between G6Sulfur and G6Solar provide insight on the potential impact of
438 stratospheric sulfate aerosols on fires other than the intended climate intervention. In general, using
439 sulfur to create climate control enhances the effect of the solar management on the modeled fire
440 response. While both geoengineering approaches show strongest inverse relationships between fire
441 parameters and relative humidity and soil moisture, G6Sulfur shows smaller reductions in these
442 climate variables than G6Solar. Globally, G6Sulfur has lower burned area and fire carbon
443 emissions than G6Solar by the end of the century. The differences between G6Sulfur and G6Solar
444 varies regionally (Figures 7a-7b). For example, over most regions, G6Sulfur has less fire activity
445 than G6Solar whereas over Europe, G6Sulfur has more fire activity than G6Solar, which is related
446 to the warming over Northern Eurasia caused by G6Sulfur (Figure 7c) and a positive correlation
447 between BA and surface temperature over Europe. However, we note that two ensemble members
448 may not fully reflect the robust signal. The spatial distributions of differences between G6Sulfur
449 and G6Solar in burned area and fire carbon emissions (Figures 7a-7b) are close to the spatial
450 distributions of difference between G6Sulfur and G6Solar in relative humidity (Figure 7e) and soil
451 water content (Figure 7g). G6Sulfur has higher relative humidity and soil water content over most
452 regions. However, over Europe relative humidity and soil water content in G6Sulfur are lower than
453 those in G6Solar, which is consistent with what has been found in burned area and fire carbon
454 emissions. In addition, over South America, the distribution of difference in relative humidity and
455 soil water content is similar to the distribution of difference in burned area and fire carbon
456 emissions. This indicate that the differences in future fire activity between the two geoengineering
457 approaches is likely driven by relative humidity and soil water content.

458 A summary of the relationships between ΔBA and the changes in the related variables (ΔTS ,
459 $\Delta Precip$, ΔRH , $\Delta U10$, $\Delta SOILWATER$, and $\Delta FSDS$) for G6Sulfur versus G6Solar is shown in
460 Figure 8 (note that ΔBA as well as Δ of other variables are calculated by the difference of the
461 geoengineering run from the reference case, i.e., SSP5-8.5). Overall, the impacts of these driving
462 variables are similar in the two geoengineering approaches (as the points fall close to the diagonal).



463 However, these variables in general have larger impacts on burned area in G6Solar than in
464 G6Sulfur (as the majority of the points fall in the shaded area where the x-axis value is larger than
465 the y-axis value). This is expected since the climate impacts of solar irradiance reduction (G6Solar)
466 is more direct than that of stratospheric sulfate aerosols (G6Sulfur) and stratospheric sulfate
467 aerosols can yield to additional changes (such as higher diffuse radiation that benefits plant
468 growth). This is consistent with that G6Sulfur has slightly higher total vegetation carbon than
469 G6Solar or SSP5-8.5, even though this difference is relatively small compared to the difference
470 caused by CO₂ (Figure 4g).

471 **4.8 Discussion**

472 The key finding of this study is that fire burned area and emissions are lower in the
473 geoengineering runs than not only SSP5-8.5 but also the target SSP2-4.5 run in CESM2/WACCM6.
474 Here we analyze the key climate variables that are largely and/or directly impacted by the two
475 geoengineering approaches and are important drivers of fires. A summary of the relationships
476 between Δ BA and the change in the related variables (Δ TS, Δ Precip, Δ RH, Δ U10, Δ SOILWATER,
477 and Δ FSDS) versus the relationships between Δ Cemis and the change in the related variables for
478 G6Solar, G6Sulfur, and SSP2-4.5 are shown in Figure 9. The future trends of the analyzed
479 variables and their changes from SSP5-8.5 can be opposite over different regions. However, the
480 directions of impact (i.e., positive or negative correlation) are overall consistent across the 14 fire
481 regions and 3 scenarios. Therefore the dominant factors are also different across regions.

482 We note that under both geoengineering scenarios, changes in relative humidity, soil water,
483 and downwelling solar flux at the surface all have strongest impacts over Equatorial Asia (as
484 shown by strongest correlations among the 14 regions; Figure 9). Changes in wind speed and
485 precipitation also have relative strong impacts over Equatorial Asia compared to other regions.
486 Overall, Equatorial Asia is the most sensitive to the climate variable changes introduced by both
487 geoengineering approaches (Figure 9), even though the resulting fire activity changes over
488 Equatorial Asia are not as strong as some other regions (Figure 3) likely due to the relatively weak
489 change in the climate variables (e.g., Figures 5). On the contrary, Boreal North America is not
490 sensitive to most of the climate variable changes introduced by both geoengineering approaches
491 (the correlations are the lowest and close to 0, Figure 9), which is likely the reason why the 40°N–
492 70°N latitude band is the only latitude band in which the zonal mean burned area consistently
493 increases even under the geoengineering scenarios (Figures 1 and 2). Boreal Asia is similar to
494 Boreal North America with the correlations overall being slightly stronger.

495 For G6Solar and G6Sulfur, the impacts of the shown variables (especially for Δ TS, Δ RH,
496 Δ U10, and Δ FSDS) on burned area are in general stronger than their impacts on fire carbon
497 emissions (as shown by more data points that fall into the shaded area). This is expected because
498 these variables first impact burned area, and then fire carbon emissions are determined by burned
499 area and fuel availability. Fuel availability is further directly or indirectly impacted by many other
500 variables including the shown ones here, which introduce more uncertainties. The patterns in
501 G6Solar and G6Sulfur and closer to each other when using SSP2-4.5 as a reference (Figures 6).
502 This is not only because their approaches to reducing forcing from SSP5-8.5 to 4.5 W/m² are
503 different, but also because the scenario configuration of SSP2-4.5 is different from SSP5-8.5 and
504 SSP5-8.5-based G6Solar and G6Sulfur (e.g., LULCC).



505 The analyses above (Sections 4.1-4.7) use SSP5-8.5 as the reference case to calculate the
506 changes (Δ) because the two geoengineering scenarios are based on SSP5-8.5, and their difference
507 is only due to the geoengineering approaches. Here we also include analyses that uses the target
508 SSP2-4.5 as the reference case in the Supplement (Figures S13). The signs of the correlations are
509 in general consistent whether SSP5-8.5 or SSP2-4.5 is used as the reference case (Figures S14-
510 S15). For example, even though relative humidity change from SSP2-4.5 are very different
511 regionally under G6Solar and G6Sulfur (Figure 5), the signs of the correlations are consistently
512 negative over all regions and under the two geoengineering scenarios. In general, the impacts of
513 the analyzed variables on changes of the burned area and fire carbon emissions from SSP2-4.5 are
514 weaker (Figures S14-S15), likely due to the fact that the changes (Δ) between the two
515 geoengineering scenarios and SSP2-4.5 are due to not only geoengineering introduced climate
516 variable changes (e.g., surface temperature, relative humidity, soil water content, etc.) but also
517 other factors such as atmospheric CO₂ and LULCC.

518 **4.9 Uncertainty and limitation**

519 We recognize that there are several limitations in this study. For example, even though
520 CESM2 is a state-of-the-art model, uncertainties and limitations exist in the model
521 parameterizations (including the parameterization of fire-related processes and the lack of
522 interactive fire emissions). In addition, the fire emissions of trace gases and aerosols are not fully
523 coupled, as CESM2 uses the CMIP6 fire emission inventories. This study analyzes results from
524 only one model (CESM2) and similar studies need to be conducted with other models to test inter-
525 model consistency. Lastly, there are only two ensemble members in each geoengineering scenario,
526 which can lead to larger variability at regional scale in particular resulting in large uncertainties in
527 the response of geoengineering on rainfall with implications of other relevant variables. While
528 largescale changes are significant, a larger ensemble size in future study will reduce uncertainties
529 in the regional results. More studies are needed to fully understand the future trends of fires and
530 the impact of geoengineering on fires.

531 **4. Conclusions**

532 Here we analyzed the future fires under geoengineering as well as SSP scenarios, and
533 assess how the different geoengineering approaches impact fires. The major conclusions and
534 implications are as follows:

535 (1) The global total wildfire burned area is projected to increase under the unmitigated scenario
536 (SSP5-8.5), and decrease under the two geoengineering scenarios (solar irradiance reduction and
537 stratospheric sulfate aerosols) in the 21st century.

538 (2) By the end of the century, the two geoengineering scenarios exhibit lower burned area and fire
539 carbon emissions than not only their base-forcing scenario (SSP5-8.5) but also the targeted-forcing
540 scenario (SSP2-4.5).

541 (3) The two geoengineering approaches (solar irradiance reduction and stratospheric sulfate
542 aerosols) generally lead to less wildfire activity in most regions in 2091-2100, except for the
543 Northern Hemisphere Africa and Equatorial Asia. The 40°N–70°N latitude band is the only
544 latitude band in which the zonal mean burned area consistently increases under all the scenarios,
545 even the geoengineering scenarios.



546 (4) Overall, changes of G6Solar and G6Sulfur from SSP5-8.5 in surface temperature, wind speed,
547 and downwelling solar flux at the surface are positively correlated to the changes in burned area
548 and fire carbon emissions, while their changes in precipitation, relative humidity, and soil water
549 content are negatively correlated to the changes in burned area and fire carbon emissions.

550 (5) Generally, the stratospheric sulfate aerosols approach has a stronger fire-reducing effect than
551 the solar irradiance reduction approach. The impacts of the analyzed variable changes are generally
552 larger (percent-wise) on burned area than fire carbon emissions.

553 (6) Geoengineering imposed reduction in surface temperature and wind speed, and increase in
554 relative humidity and soil moisture, reduce fires by the end of the century. However, the reduction
555 in precipitation resulting from geoengineering offsets its overall fire-reducing effect to some extent.

556 The success of future fire mitigation with the two geoengineering approaches in the
557 CESM2/WACCM6 model results is encouraging. However, this study is not a closure study due
558 to the uncertainties and limitations (Section 4.9). More research is needed for this topic. Here we
559 do not indicate that fewer fires under the geoengineering approaches are definitively beneficial.
560 After all, fire is a natural process and a key component of the dynamic Earth system, and wildfires
561 were present long before anthropogenic activities. Lastly, fire risk increase is only one of many
562 possible consequences of climate change, and fire activity reduction is also only one of many
563 possible consequences of climate intervention. We present this study only as a reference for the
564 future when geoengineering is considered.

565

566 **Data availability**

567 The simulation data used in this study are archived on the Earth System Grid Federation (ESGF)
568 (<https://esgf-node.llnl.gov/projects/cmip6>; last access: 12 December 2022). The model Source ID
569 is CESM2-WACCM for CESM2-WACCM6. FINN2.5 data are available at:
570 <https://www.acom.ucar.edu/Data/fire/>. GFED data are available at:
571 <https://www.globalfiredata.org/>.

572

573 **Author contributions**

574 WT led the analysis with the contribution from ST. ST and DML contributed to the interpretation
575 of the model results. WT prepared the paper with improvements from ST, DML, FL, CH, LKE,
576 RRB, and LX.

577

578 **Acknowledgements**

579 This material is based upon work supported by the National Center for Atmospheric Research,
580 which is a major facility sponsored by the National Science Foundation under Cooperative
581 Agreement No. 1852977. Wenfu Tang was supported by NCAR Advanced Study Program
582 Postdoctoral Fellowship. W. Tang thanks Wangcai Bao (Syrian hamster; Sep 8, 2020 – Jul 22,
583 2022) for his support during the pandemic.

584

585

586

587

587 **References**

588 Abatzoglou, J. T., Williams, A. P., & Barbero, R. (2019). Global emergence of anthropogenic
589 climate change in fire weather indices. *Geophysical Research Letters*, 46(1), 326-336.



- 590 Andela, N. and van der Werf, G.R., 2014. Recent trends in African fires driven by cropland
591 expansion and El Nino to La Nina transition. *Nature Climate Change*, 4(9), pp.791-795.
- 592 Andela N, Morton DC, Giglio L, Chen Y, Van Der Werf GR, Kasibhatla PS, DeFries RS, Collatz
593 GJ, Hantson S, Kloster S, Bachelet D. A human-driven decline in global burned area. *Science*.
594 2017 Jun 30;356(6345):1356-62.
- 595 Bowman, D.M., Balch, J.K., Artaxo, P., Bond, W.J., Carlson, J.M., Cochrane, M.A., D'Antonio,
596 C.M., DeFries, R.S., Doyle, J.C., Harrison, S.P. and Johnston, F.H., 2009. Fire in the Earth system.
597 *science*, 324(5926), pp.481-484.
- 598 Bowman, D. M. J. S., Balch, J. K., Artaxo, P., Bond, W. J., Carlson, J. M., Cochrane, M. A.,
599 D'Antonio, C. M., DeFries, R. S., Doyle, J. C., Harrison, S. P., Johnston, F. H., Keeley, J. E., Ford,
600 B., Val Martin, M., Zelasky, S. E., Fischer, E. V., Anenberg, S. C., Heald, C. L., and Pierce, J. R.:
601 Future Fire Impacts on Smoke Concentrations, Visibility, and Health in the Contiguous United
602 States, *GeoHealth*, 2, 229–247, 2018.
- 603 Bowman, D. M. J. S., Kolden, C. A., Abatzoglou, J. T., Johnston, F. H., van der Werf, G. R., &
604 Flannigan, M. (2020). Vegetation fires in the Anthropocene. *Nature Reviews Earth & Environment*,
605 1-16.
- 606 Brey, S. J., Barnes, E. A., Pierce, J. R., Wiedinmyer, C., & Fischer, E. V. (2018). Environmental
607 conditions, ignition type, and air quality impacts of wildfires in the southeastern and western
608 United States. *Earth's Future*, 6(10), 1442-1456.
- 609 Brey, S. J., Barnes, E. A., Pierce, J. R., Swann, A. L., & Fischer, E. V. Past variance and future
610 projections of the environmental conditions driving western US summertime wildfire burn area.
611 *Earth's Future*, e2020EF001645, 2020.
- 612 Chen, Y., Morton, D. C., Andela, N., Van Der Werf, G. R., Giglio, L., & Randerson, J. T. (2017).
613 A pan-tropical cascade of fire driven by El Niño/Southern Oscillation. *Nature Climate Change*,
614 7(12), 906-911.
- 615 Coen, J., Cameron, M., Michalakes, J., Patton, E., Riggan, P., and Yedinak, K.: WRF-Fire:
616 Coupled weather-wildland fire modeling with the Weather Research and Forecasting model, *J.*
617 *Appl. Meteor. Climatol.*, 52, 16–38, doi:10.1175/JAMC-D-12-023.1, 2013.
- 618 Danabasoglu, G., Lamarque, J. F., Bacmeister, J., Bailey, D. A., DuVivier, A. K., Edwards, J.,
619 Emmons, L. K., Fasullo, J., Garcia, R., Gettelman, A., Hannay, C., Holland, M. M., Large, W. G.,
620 Lauritzen, P. H., Lawrence, D. M., Lenaerts, J. T. M., Lindsay, K., Lipscomb, W. H., Mills, M. J.,
621 Neale, R., Oleson, K. W., OttoBliesner, B., Phillips, A. S., Sacks, W., Tilmes, S., van Kampenhout,
622 L., Vertenstein, M., Bertini, A., Dennis, J., Deser, C., Fischer, C., Fox-Kemper, B., Kay, J. E.,
623 Kinnison, D., Kushner, P. J., Larson, V. E., Long, M. C., Mickelson, S., Moore, J. K., Nienhouse,
624 E., Polvani, L., Rasch, P. J., and Strand, W. G.: The Community Earth System Model Version 2
625 (CESM2), *J. Adv. Model. Earth Syst.*, 12, 1–35, <https://doi.org/10.1029/2019MS001916>, 2020.
- 626 Di Virgilio, G., Evans, J. P., Blake, S. A. P., Armstrong, M., Dowdy, A. J., Sharples, J., & McRae,
627 R.: Climate change increases the potential for extreme wildfires. *Geophysical Research Letters*,
628 46, 8517–8526. <https://doi.org/10.1029/2019GL083699>, 2019.
- 629 Di Virgilio G, Evans JP, Clarke H, Sharples J, Hirsch AL, Hart MA. Climate change significantly
630 alters future wildfire mitigation opportunities in southeastern Australia. *Geophysical Research*
631 *Letters*. 2020 Aug 16;47(15):e2020GL088893.



- 632 Emmons, L. K., Schwantes, R. H., Orlando, J. J., Tyndall, G., Kinnison, D., Lamarque, J.-F.,
633 Marsh, D., Mills, M. J., Tilmes, S., Bardeen, Ch., Buchholz, R. R., Conley, A., Gettelman, A.,
634 Garcia, R., Simpson, I., Blake, D. R., Meinardi, S., and Pétron, G.: The Chemistry Mechanism in
635 the Community Earth System Model version 2 (CESM2), *J. Adv. Model. Earth Sys.*, 12,
636 e2019MS001882, <https://doi.org/10.1029/2019MS001882>, 2020.
- 637 Flannigan M, Campbell I, Wotton M, Carcaillet C, Richard P, Bergeron Y. Future fire in Canada's
638 boreal forest: paleoecology results and general circulation model-regional climate model
639 simulations. *Canadian journal of forest research*. 2001 May 1;31(5):854-64.
- 640 Flannigan, M. D., Krawchuk, M. A., de Groot, W. J. et al.: Implications of changing climate for
641 global wildland fire, *Int. J. Wildland Fire*, 18, 483–507, 2009.
- 642 Flannigan, M., Cantin, A. S., De Groot, W. J., Wotton, M., Newbery, A., & Gowman, L. M.:
643 Global wildland fire season severity in the 21st century. *Forest Ecology and Management*, 294,
644 54-61, 2013.
- 645 Ford B, Val Martin M, Zelasky SE, Fischer EV, Anenberg SC, Heald CL, Pierce JR. Future fire
646 impacts on smoke concentrations, visibility, and health in the contiguous United States. *GeoHealth*.
647 2018 Aug;2(8):229-47.
- 648 Gettelman, A., Mills, M. J., Kinnison, D. E., Garcia, R. R., Smith, A. K., Marsh, D. R., Tilmes, S.,
649 Vitt, F., Bardeen, C. G., McInerney, J., Liu, H.-L., Solomon, S. C., Polvani, L. M., Emmons, L. K.,
650 Lamarque, J.-F., Richter, J. H., Glanville, A. S., Bacmeister, J. T., Phillips, A. S., Neale, R. B.,
651 Simpson, I. R., DuVivier, A. K., Hodzic, A., and Randel, W. J.: The Whole Atmosphere
652 Community Climate Model Version 6 (WACCM6), *Journal of Geophysical Research:*
653 *Atmospheres*, <https://doi.org/10.1029/2019JD030943>, 2019.
- 654 Girardin MP, Mudelsee M. Past and future changes in Canadian boreal wildfire activity.
655 *Ecological Applications*. 2008;18(2):391-406.
- 664 Giglio, L., Randerson, J. T., van der Werf, G. R., Kasibhatla, P. S., Collatz, G. J., Morton, D. C.,
665 and DeFries, R. S.: Assessing variability and long-term trends in burned area by merging multiple
666 satellite fire products, *Biogeosciences*, 7, 1171–1186, <https://doi.org/10.5194/bg-7-1171-2010>,
667 2010.
- 668 Hanes, C. C., Wang, X., Jain, P., Parisien, M. A., Little, J. M., & Flannigan, M. D. (2019). Fire-
669 regime changes in Canada over the last half century. *Canadian Journal of Forest Research*, 49(3),
670 256-269.
- 671 Huang Y, Jin Y, Schwartz MW, Thorne JH. Intensified burn severity in California's northern
672 coastal mountains by drier climatic condition. *Environmental Research Letters*. 2020 Sep
673 25;15(10):104033.
- 674 Hurtt, G.C., L. Chini. R. Sahajpal, S. Frolking, B.L. Boudris, K. Calvin, J.C. Doelman, J. Fisk, S.
675 Fujimori, K.K. Goldewijk, T. Hasegawa, P. Havlik, A. Henimann, F. Humpnoeder, J. Jungclaus, J.
676 Kaplan, J. Kennedy, T. Kristzin, D. Lawrence, P. Lawrence, L. Ma, O. Mertz, J. Pongratz, A. Popp,
677 B. Poulter, K. Riahi, E. Shevliakova, E. Stehfest, P. Thornton, F.N. Tubiello, D.P. Van Vuuren,
678 and X. Zhang, 2020. Harmonization of Global Land-Use Change and Management for the Period
679 850-2100 (LUH2) for CMIP6. *GMD*, 13, 5425-5464, doi.org/10.5194/gmd-13-5425-2020.



- 680 Jiang, J., Cao, L., MacMartin, D. G., Simpson, I. R., Kravitz, B., Cheng, W., Visioni, D., Tilmes,
681 S., Richter, J. H., and Mills, M. J.: Stratospheric Sulfate Aerosol Geoengineering Could Alter the
682 High-Latitude Seasonal Cycle, *Geophys. Res. Lett.*, 46, 14153–14163,
683 <https://doi.org/10.1029/2019GL085758>, 2019.
- 684 Jones, B. and O’Neill, B. C.: Spatially explicit global population scenarios consistent with the
685 Shared Socioeconomic Pathways, *Environ. Res. Lett.*, 11, 4003, <https://doi.org/10.1088/1748-9326/11/8/084003>, 2016.
- 687 Jones, A., Haywood, J. M., Jones, A. C., Tilmes, S., Kravitz, B., and Robock, A.: North Atlantic
688 Oscillation response in GeoMIP experiments G6solar and G6sulfur: why detailed modelling is
689 needed for understanding regional implications of solar radiation management, *Atmos. Chem.
690 Phys. Discuss.*, <https://doi.org/10.5194/acp-2020-802>, in review, 2020.
- 691 Krawchuk, M. A., Kull, C. A., Marston, J. B., Moritz, M. A., Prentice, I. C., Roos, C. I., Scott,
692 A. C., Swetnam, T. W., van der Werf, G. R., and Pyne, S. J.: Fire in the Earth System, *Science*,
693 324, 481–484, <https://doi.org/10.1126/science.1163886>, 2009.
- 694 Knorr, W., Arneth, A., and Jiang, L.: Demographic controls of future global fire risk, *Nat. Clim.
695 Change*, 6, 781–785, <https://doi.org/10.1038/NCLIMATE2999>, 2016a.
- 696 Knorr, W., Jiang, L., and Arneth, A.: Climate, CO₂ and human population impacts on global
697 wildfire emissions, *Biogeosciences*, 13, 267–282, <https://doi.org/10.5194/bg-13-267-2016>, 2016b.
- 698 Kravitz, B., Robock, A., Tilmes, S., Boucher, O., English, J. M., Irvine, P. J., Jones, A., Lawrence,
699 M. G., MacCracken, M., Muri, H., Moore, J. C., Niemeier, U., Phipps, S. J., Sillmann, J.,
700 Storelvmo, T., Wang, H., and Watanabe, S.: The Geoengineering Model Intercomparison Project
701 Phase 6 (GeoMIP6): simulation design and preliminary results, *Geosci. Model Dev.*, 8, 3379–3392,
702 [doi:10.5194/gmd-8-3379-2015](https://doi.org/10.5194/gmd-8-3379-2015), 2015.
- 703 Kravitz, B., Lamarque, J.-F., Tribbia, J. J., Tilmes, S., Vitt, F., Richter, J. H., MacMartin, D. G.,
704 and Mills, M. J.: First Simulations of Designing Stratospheric Sulfate Aerosol Geoengineering to
705 Meet Multiple Simultaneous Climate Objectives, *J. Geophys. Res.-Atmos.*, 122, 12616–12634,
706 <https://doi.org/10.1002/2017jd026874>, 2017.
- 707 Lasslop, G., Hantson, S., Harrison, S. P., Bachelet, D., Burton, C., Forkel, M., Forrest, M., Li F.,
708 Melton, J. R., Yue, C., Archibald, S., Scheiter, S., Arneth, A., Hickler, T., and Sitch, S.: Global
709 ecosystems and fire: Multi-model assessment of fire-induced tree-cover and carbon storage
710 reduction, *Glob. Change Biol.*, 26, 5027–5041, <https://doi.org/10.1111/gcb.15160>, 2020.
- 711 Lawrence, D. M., Hurtt, G. C., Arneth, A., Brovkin, V., Calvin, K. V., Jones, A. D., Jones, C. D.,
712 Lawrence, P. J., de Noblet-Ducoudré, N., Pongratz, J., Seneviratne, S. I., and Shevliakova, E.: The
713 Land Use Model Intercomparison Project (LUMIP) contribution to CMIP6: rationale and
714 experimental design, *Geosci. Model Dev.*, 9, 2973–2998, <https://doi.org/10.5194/gmd-9-2973-2016>, 2016.
- 716 Lawrence, D. M., Fisher, R. A., Koven, C. D., Oleson, K. W., Swenson, S. C., Bonan, G., Collier,
717 N., Ghimire, B., van Kampenhout, L., Kennedy, D., Kluzek, E., Lawrence, P. J., Li, F., Li, H.,
718 Lombardozzi, D., Riley, W. J., Sacks, W. J., Shi, M., Vertenstein, M., Wieder, W. R., Xu, C., Ali,
719 A. A., Badger, A. M., Bisht, G., Brunke, M. A., Burns, S. P., Buzan, J., Clark, M., Craig, A.,
720 Dahlin, K., Drewniak, B., Fisher, J. B., Flanner, M., Fox, A. M., Gentine, P., Hoffman, F., Keppel-
721 Aleks, G., Knox, R., Kumar, S., Lenaerts, J., Leung, L. R., Lipscomb, W. H., Lu, Y., Pandey, A.,



- 722 Pelletier, J. D., Perket, J., Randerson, J. T., Ricciuto, D. M., Sanderson, B. M., Slater, A., Subin,
723 Z. M., Tang, J., Thomas, R. Q., Val Martin, M., and Zeng, X.: The Community Land Model version
724 5: Description of new features, benchmarking, and impact of forcing uncertainty. *Journal of*
725 *Advances in Modeling Earth Systems*, 11(12), 4245–4287, 2019.
- 726 Le Goff H, Flannigan MD, Bergeron Y. Potential changes in monthly fire risk in the eastern
727 Canadian boreal forest under future climate change. *Canadian journal of forest research*. 2009
728 Dec;39(12):2369-80.
- 729 Li, F., Zeng, X. D., and Levis, S.: A process-based fire parameterization of intermediate
730 complexity in a Dynamic Global Vegetation Model, *Biogeosciences*, 9, 2761–2780,
731 <https://doi.org/10.5194/bg-9-2761-2012>, 2012.
- 732 Li, F., Levis, S., and Ward, D. S.: Quantifying the role of fire in the Earth system – Part 1: Improved
733 global fire modeling in the Community Earth System Model (CESM1), *Biogeosciences*, 10, 2293–
734 2314, <https://doi.org/10.5194/bg-10-2293-2013>, 2013.
- 735 Li, F. and Lawrence, D. M.: Role of fire in the global land water budget during the 20th century
736 through changing ecosystems, *J. Climate*, 30, 1893–908, 2017.
- 737 Li, F., Lawrence, D. M., and Bond-Lamberty, B.: Impact of fire on global land surface air
738 temperature and energy budget for the 20th century due to changes within ecosystems, *Environ.*
739 *Res. Lett.*, 12, <https://doi.org/10.1088/1748-9326/aa6685>, 2017.
- 740 Li, F., Lawrence, D. M., and Bond-Lamberty, B.: Human impacts on 20th century fire dynamics
741 and implications for global carbon and water trajectories, *Global Planet. Change*, 162, 18–27, 2018.
- 742 Li, F., Val Martin, M., Andreae, M. O., Arneth, A., Hantson, S., Kaiser, J. W., Lasslop, G., Yue,
743 C., Bachelet, D., Forrest, M., Kluzek, E., Liu, X., Mangeon, S., Melton, J. R., Ward, D. S.,
744 Darmenov, A., Hickler, T., Ichoku, C., Magi, B. I., Sitch, S., van der Werf, G. R., Wiedinmyer, C.,
745 and Rabin, S. S.: Historical (1700–2012) global multi-model estimates of the fire emissions from
746 the Fire Modeling Intercomparison Project (FireMIP), *Atmos. Chem. Phys.*, 19, 12545–12567,
747 <https://doi.org/10.5194/acp-19-12545-2019>, 2019.
- 748 Li, Y., Mickley, L. J., Liu, P., and Kaplan, J. O.: Trends and spatial shifts in lightning fires and
749 smoke concentrations in response to 21st century climate over the national forests and parks of the
750 western United States, *Atmos. Chem. Phys.*, 20, 8827–8838, [https://doi.org/10.5194/acp-20-8827-](https://doi.org/10.5194/acp-20-8827-2020)
751 2020, 2020.
- 752 Li F., D. Lawrence, Y.-Q. Jiang, X.-H. Liu, and Z.-D. Lin, 2022: Fire aerosols slow down the
753 global water cycle, *J. Climate*, [https://journals.ametsoc.org/view/journals/clim/aop/JCLI-D-21-](https://journals.ametsoc.org/view/journals/clim/aop/JCLI-D-21-0817.1/JCLI-D-21-0817.1.xml)
754 0817.1/JCLI-D-21-0817.1.xml.
- 755 Liu, Y. Q., Stanturf, J., and Goodrick, S.: Trends in global wildfire potential in a changing climate,
756 *Forest Ecol. Manag.*, 259, 685–697, <https://doi.org/10.1016/j.foreco.2009.09.002>, 2010.
- 757 Liu, Z., Ballantyne, A. P., & Cooper, L. A. (2019). Biophysical feedback of global forest fires on
758 surface temperature. *Nature communications*, 10(1), 1–9.
- 759 Loehman, R. A. (2020). Drivers of wildfire carbon emissions. *Nature Climate Change*, 1–2.
- 760 Luo, L. F., Tang, Y., Zhong, S. Y., Bian, X. D., and Heilman, W. E.: Will Future Climate Favor
761 More Erratic Wildfires in the Western United States?, *J. Appl. Meteorol. Climatol.*, 52, 2410–2417,
762 <https://doi.org/10.1175/jamc-d-12-0317.1>, 2013.



- 763 Meehl, G. A., Arblaster, J. M., Bates, S., Richter, J. H., Tebaldi, C., Gettelman, A., et al.
764 (2020). Characteristics of future warm er basestates in CESM2. *Earth and Sp aceScience*, 7,
765 e2020EA001296. <https://doi.org/10.1029/2020EA001296>.
- 766 Riahi, K., van Vuuren, D. P., Kriegler, E., Edmonds, J., O'Neill, B. C., Fujimori, S., Bauer, N.,
767 Calvin, K., Dellink, R., Fricko, O., Lutz, W., Popp, A., Cuaresma, J. C., KC, S., Leimbach, M.,
768 Jiang, L., Kram, T., Rao, S., Emmerling, J., Ebi, K., Hasegawa, T., Havlik, P., Humpenöder, F.,
769 Da Silva, L. A., Smith, S., Stehfest, E., Bosetti, V., Eom, J., Gernaat, D., Masui, T., Rogelj, J.,
770 Strefler, J., Drouet, L., Krey, V., Luderer, G., Harmsen, M., Takahashi, K., Baumstark, L.,
771 Doelman, J. C., Kainuma, M., Klimont, Z., Marangoni, G., Lotze-Campen, H., Obersteiner, M.,
772 Tabeau, A., and Tavoni, M.: The Shared Socioeconomic Path ways and their energy, land use, and
773 greenhouse gas emissions implications: An overview, *Global Environ. Chang.*, 42, 153– 168,
774 <https://doi.org/10.1016/j.gloenvcha.2016.05.009>, 2017.
- 775 Richter, J. H., Tilmes, S., Mills, M. J., Tribbia, J. J., Kravitz, B., Macmartin, D. G., Vitt, F., and
776 Lamarque, J. F.: Stratospheric dynamical response and ozone feedbacks in the presence of SO₂
777 injections, *J. Geophys. Res.-Atmos.*, 122, 12557–12573, <https://doi.org/10.1002/2017JD026912>,
778 2017.
- 779 Robock A. Benefits and risks of stratospheric solar radiation management for climate intervention
780 (geoengineering). *Bridge*. 2020 Mar 1;50(1):59-67.
- 781 O'Neill, B. C., Tebaldi, C., van Vuuren, D. P., Eyring, V., Friedlingstein, P., Hurtt, G., Knutti, R.,
782 Kriegler, E., Lamarque, J.-F., Lowe, J., Meehl, G. A., Moss, R., Riahi, K., and Sanderson, B. M.:
783 The Scenario Model Intercomparison Project (ScenarioMIP) for CMIP6, *Geosci. Model Dev.*, 9,
784 3461–3482, <https://doi.org/10.5194/gmd-9-3461-2016>, 2016.
- 785 O'Neill BC, Kriegler E, Ebi KL, Kemp-Benedict E, Riahi K, Rothman DS, van Ruijven BJ, van
786 Vuuren DP, Birkmann J, Kok K, Levy M. The roads ahead: Narratives for shared socioeconomic
787 pathways describing world futures in the 21st century. *Global environmental change*. 2017 Jan
788 1;42:169-80.
- 789 Pechony, O. and Shindell, D.: Driving forces of global wildfires over the past millennium and the
790 forthcoming century, *P. Natl. Acad. Sci. USA*, 107, 19167–19170, doi:10.1073/pnas.1003669107,
791 2010.
- 792 Pitman AJ, Narisma GT, McAnaney J. The impact of climate change on the risk of forest and
793 grassland fires in Australia. *Climatic Change*. 2007 Oct 1;84(3-4):383-401.
- 794 Randerson, J.T., G.R. van der Werf, L. Giglio, G.J. Collatz, and P.S. Kasibhatla. 2018. Global Fire
795 Emissions Database, Version 4.1 (GFEDv4). ORNL DAAC, Oak Ridge, Tennessee, USA.
796 <https://doi.org/10.3334/ORNLDAAC/1293>.
- 797 Rey, D. M., Walvoord, M. A., Minsley, B. J., Ebel, B. A., Voss, C. I., & Singha, K. (2020).
798 Wildfire-Initiated Talik development exceeds current thaw projections: Observations and models
799 from Alaska's continuous permafrost zone. *Geophysical Research Letters*, 47,
800 e2020GL087565. <https://doi.org/10.1029/2020GL087565>.
- 801 Shiogama, H., Hirata, R., Hasegawa, T., Fujimori, S., Ishizaki, N. N., Chatani, S., Watanabe, M.,
802 Mitchell, D., and Lo, Y. T. E.: Historical and future anthropogenic warming effects on droughts,



- 803 fires and fire emissions of CO₂ and PM_{2.5} in equatorial Asia when 2015-like El Niño events occur,
804 *Earth Syst. Dynam.*, 11, 435–445, <https://doi.org/10.5194/esd-11-435-2020>, 2020.
- 805 Simpson, I., Tilmes, S., Richter, J., Kravitz, B., MacMartin, D., Mills, M., Fasullo, J., and
806 Pendergrass, A.: The regional hydroclimate response to stratospheric sulfate geoengineering and
807 the role of stratospheric heating, *J. Geophys. Res.-Atmos.*, 124, 2019JD031093,
808 <https://doi.org/10.1029/2019JD031093>, 2019.
- 809 Stralberg D, Wang X, Parisien MA, Robinne FN, Sólymos P, Mahon CL, Nielsen SE, Bayne EM.
810 Wildfire-mediated vegetation change in boreal forests of Alberta, Canada. *Ecosphere*. 2018
811 Mar;9(3):e02156.
- 812 Tang et al., Effects of fire diurnal variation and plume rise on U.S. air quality during FIREX-AQ
813 and WE-CAN based on the Multi-Scale Infrastructure for Chemistry and Aerosols (MUSICAv0),
814 *JGR-Atmosphere*, 2022, <https://doi.org/10.1029/2022JD036650>.
- 815 Tilmes, S., Garcia, R. R., Kinnison, D. E., Gettelman, A., and Rasch, P. J.: Impact of
816 geoengineered aerosols on the troposphere and stratosphere, *J. Geophys. Res.*, 114, D12305,
817 <https://doi.org/10.1029/2008JD011420>, 2009.
- 818 Tilmes S, Fasullo J, Lamarque JF, Marsh DR, Mills M, Alterskjær K, Muri H, Kristjánsson JE,
819 Boucher O, Schulz M, Cole JN. The hydrological impact of geoengineering in the Geoengineering
820 Model Intercomparison Project (GeoMIP). *Journal of Geophysical Research: Atmospheres*. 2013
821 Oct 16;118(19):11-036.
- 822 Tilmes, S., Richter, J. H., Kravitz, B., Macmartin, D. G., Mills, M. J., Simpson, I. R., Glanville, A.
823 S., Fasullo, J. T., Phillips, A. S., Lamarque, J. F., Tribbia, J., Edwards, J., Mickelson, S., and Ghosh,
824 S.: CESM1(WACCM) stratospheric aerosol geoengineering large ensemble project, *B. Am.*
825 *Meteorol. Soc.*, 99, 2361– 2371, <https://doi.org/10.1175/BAMS-D-17-0267.1>, 2018.
- 826 Tilmes, S., Hodzic, A., Emmons, L. K., Mills, M. J., Gettelman, A., Kinnison, D. E., ... &
827 Campuzano-Jost, P. (2019). Climate forcing and trends of organic aerosols in the Community
828 Earth System Model (CESM2). *Journal of Advances in Modeling Earth Systems*, 11(12), 4323-
829 4351.
- 830 Tilmes, S., MacMartin, D. G., Lenaerts, J. T. M., van Kampenhout, L., Muntjewerf, L., Xia, L.,
831 Harrison, C. S., Krumhardt, K. M., Mills, M. J., Kravitz, B., and Robock, A.: Reaching 1.5 and
832 2.0 °C global surface temperature targets using stratospheric aerosol geoengineering, *Earth Syst.*
833 *Dynam.*, 11, 579– 601, <https://doi.org/10.5194/esd-11-579-2020>, 2020.
- 834 Tilmes, S., MacMartin, D. G., Lenaerts, J. T. M., van Kampenhout, L., Muntjewerf, L., Xia, L.,
835 Harrison, C. S., Krumhardt, K. M., Mills, M. J., Kravitz, B., and Robock, A.: Reaching 1.5 and
836 2.0 °C global surface temperature targets using stratospheric aerosol geoengineering, *Earth Syst.*
837 *Dynam.*, 11, 579–601, <https://doi.org/10.5194/esd-11-579-2020>, 2020.
- 838 Val Martin, M., Heald, C. L., Lamarque, J.-F., Tilmes, S., Emmons, L. K., and Schichtel, B. A.:
839 How emissions, climate, and land use change will impact mid-century air quality over the United
840 States: a focus on effects at national parks, *Atmos. Chem. Phys.*, 15, 2805–2823,
841 <https://doi.org/10.5194/acp-15-2805-2015>, 2015.



- 842 Veira, A., Lasslop, G., and Kloster, S.: Wildfires in a warmer climate: emission fluxes, emission
843 heights, and black carbon concentrations in 2090–2099, *J. Geophys. Res.-Atmos.*, 121, 3195–
844 3223, 2016.
- 845 Visioni, D., MacMartin, D. G., Kravitz, B., Lee, W., Simpson, I. R., and Richter, J. H.: Reduced
846 poleward transport due to stratospheric heating under stratospheric aerosols geoengineering,
847 *Geophys. Res. Lett.*, 47, e2020GL089470, <https://doi.org/10.1029/2020GL089470>, 2020.
- 848 Visioni, D., MacMartin, D. G., Kravitz, B., Boucher, O., Jones, A., Lurton, T., Martine, M., Mills,
849 M. J., Nabat, P., Niemeier, U., Séférian, R., and Tilmes, S.: Identifying the sources of uncertainty
850 in climate model simulations of solar radiation modification with the G6sulfur and G6solar
851 Geoengineering Model Intercomparison Project (GeoMIP) simulations, *Atmos. Chem. Phys.*, 21,
852 10039–10063, <https://doi.org/10.5194/acp-21-10039-2021>, 2021a.
- 853 Visioni D, MacMartin DG, Kravitz B. Is turning down the sun a good proxy for stratospheric
854 sulfate geoengineering?. *Journal of Geophysical Research: Atmospheres*. Mar
855 16;126(5):e2020JD033952, 2021b.
- 856 van der Werf, G. R., Randerson, J. T., Giglio, L., Collatz, G. J., Kasibhatla, P. S., and Arellano Jr.,
857 A. F.: Interannual variability in global biomass burning emissions from 1997 to 2004, *Atmos.*
858 *Chem. Phys.*, 6, 3423–3441, <https://doi.org/10.5194/acp-6-3423-2006>, 2006.
- 859 van der Werf, G. R., Randerson, J. T., Giglio, L., Gobron, N., & Dolman, A. J. (2008). Climate
860 controls on the variability of fires in the tropics and subtropics. *Global Biogeochemical Cycles*,
861 22(3).
- 862 Walker, X. J., Rogers, B. M., Veraverbeke, S., Johnstone, J. F., Baltzer, J. L., Barrett, K., ... &
863 Goetz, S. (2020). Fuel availability not fire weather controls boreal wildfire severity and carbon
864 emissions. *Nature Climate Change*, 1-7.
- 865 Wang, X., Studens, K., Parisien, M. A., Taylor, S. W., Candau, J. N., Boulanger, Y., & Flannigan,
866 M. D. (2020). Projected changes in fire size from daily spread potential in Canada over the 21st
867 century. *Environmental Research Letters*, 15(10), 104048.
- 868 Ward, D. S., Kloster, S., Mahowald, N. M., Rogers, B. M., Randerson, J. T., and Hess, P. G.: The
869 changing radiative forcing of fires: global model estimates for past, present and future, *Atmos.*
870 *Chem. Phys.*, 12, 10857–10886, <https://doi.org/10.5194/acp-12-10857-2012>, 2012.
- 871 Wiedinmyer, C., Quayle, B., Geron, C., Belote, A., McKenzie, D., Zhang, X., O'Neill, S., and
872 Wynne, K. K.: Estimating emissions from fires in North America for air quality modeling, *Atmos.*
873 *Environ.*, 40, 3419–3432, doi:10.1016/j.atmosenv.2006.02.010, 2006.
- 874 Xia, L., Robock, A., Tilmes, S., and Neely III, R. R.: Stratospheric sulfate geoengineering could
875 enhance the terrestrial photosynthesis rate, *Atmos. Chem. Phys.*, 16, 1479–1489,
876 <https://doi.org/10.5194/acp-16-1479-2016>, 2016.
- 877 Xia, L., Nowack, P. J., Tilmes, S., and Robock, A.: Impacts of stratospheric sulfate geoengineering
878 on tropospheric ozone, *Atmos. Chem. Phys.*, 17, 11913–11928, <https://doi.org/10.5194/acp-17-11913-2017>, 2017.
- 880 Xu, Y., Lin, L., Tilmes, S., Dagon, K., Xia, L., Diao, C., Cheng, W., Wang, Z., Simpson, I., and
881 Burnell, L.: Climate engineering to mitigate the projected 21st-century terrestrial drying of the



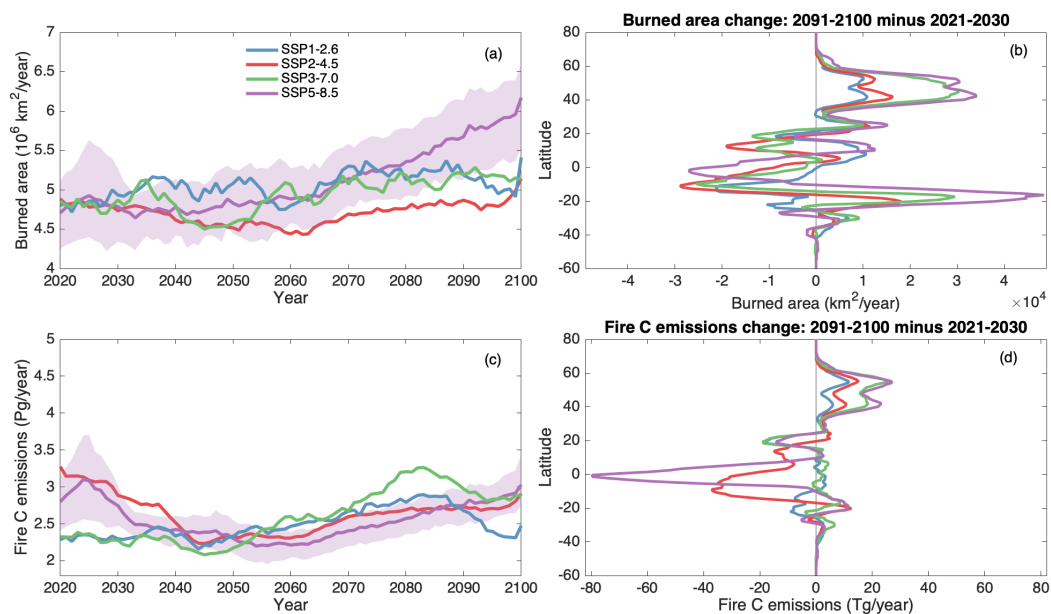
882 Americas: a direct comparison of carbon capture and sulfur injection, *Earth Syst. Dynam.*, 11,
883 673–695, <https://doi.org/10.5194/esd-11-673-2020>, 2020.

884 Yue, C., Hantson, S., Ciais, P., & Laurent, P. (2016). Evaluating FireMIP models over boreal
885 regions. *in the FireMIP 2016 Workshop*.

886 Zhang, L., W. Lau, W. Tao, and Z. Li. "Large Wildfires in the Western United States Exacerbated
887 by Tropospheric Drying Linked to a Multi-Decadal Trend in the Expansion of the Hadley
888 Circulation." *Geophysical Research Letters* 47, no. 16 (2020): e2020GL087911.

889 Zhang, Y., Fan, J., Shrivastava, M., Homeyer, C.R., Wang, Y. and Seinfeld, J.H., 2022. Notable
890 impact of wildfires in the western United States on weather hazards in the central United States.
891 *Proceedings of the National Academy of Sciences*, 119(44), p.e2207329119.

892
893

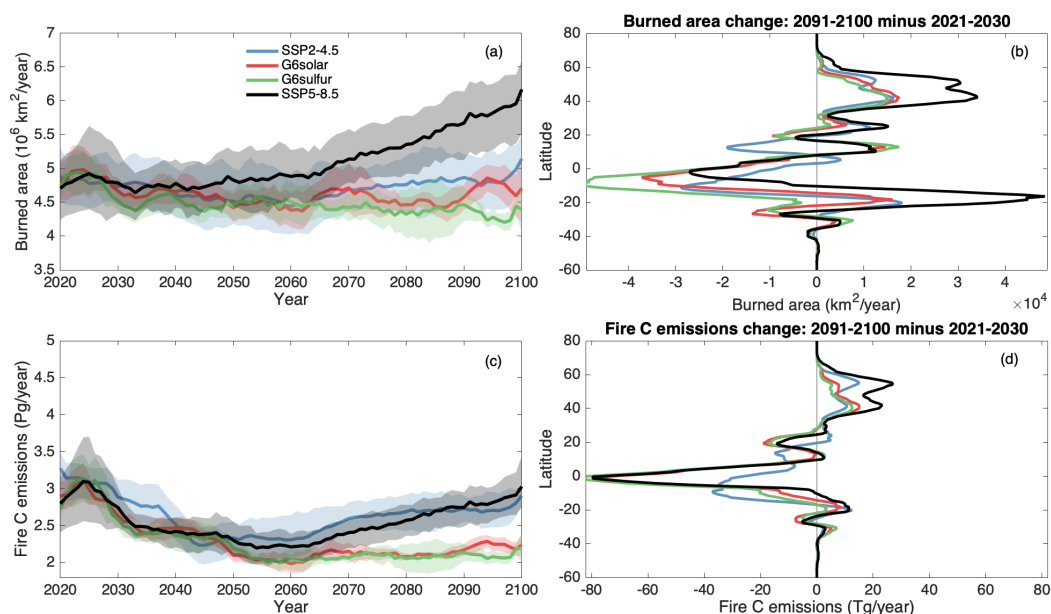


894
895
896
897
898
899
900
901
902
903
904
905
906
907

Figure 1. Overall global burned area and fire carbon emission trends and changes under SSP scenarios. (a) Time series of global burned area from 2020 to 2100 under the SSP1-2.6, SSP2-4.5, SSP3-7.0, and SSP5-8.5 scenarios (represented by different colors). For the scenarios with multiple simulations, the ranges are also shown by the shaded areas. The time series are shown as 5-year moving averages. (b) Zonal changes (absolute value) of burned area in the period 2091-2100 relative to the period 2021-2030 (calculated by the value in 2091-2100 minus the value in 2021-2030), under the SSP1-2.6, SSP2-4.5, SSP3-7.0, and SSP5-8.5 scenarios (represented by different colors, color code is the same as it in panel a). 5-degree moving average were applied to the shown zonal changes. Panels (c) and (d) are similar to panels (a) and (b), respectively, but for fire carbon emissions.



908

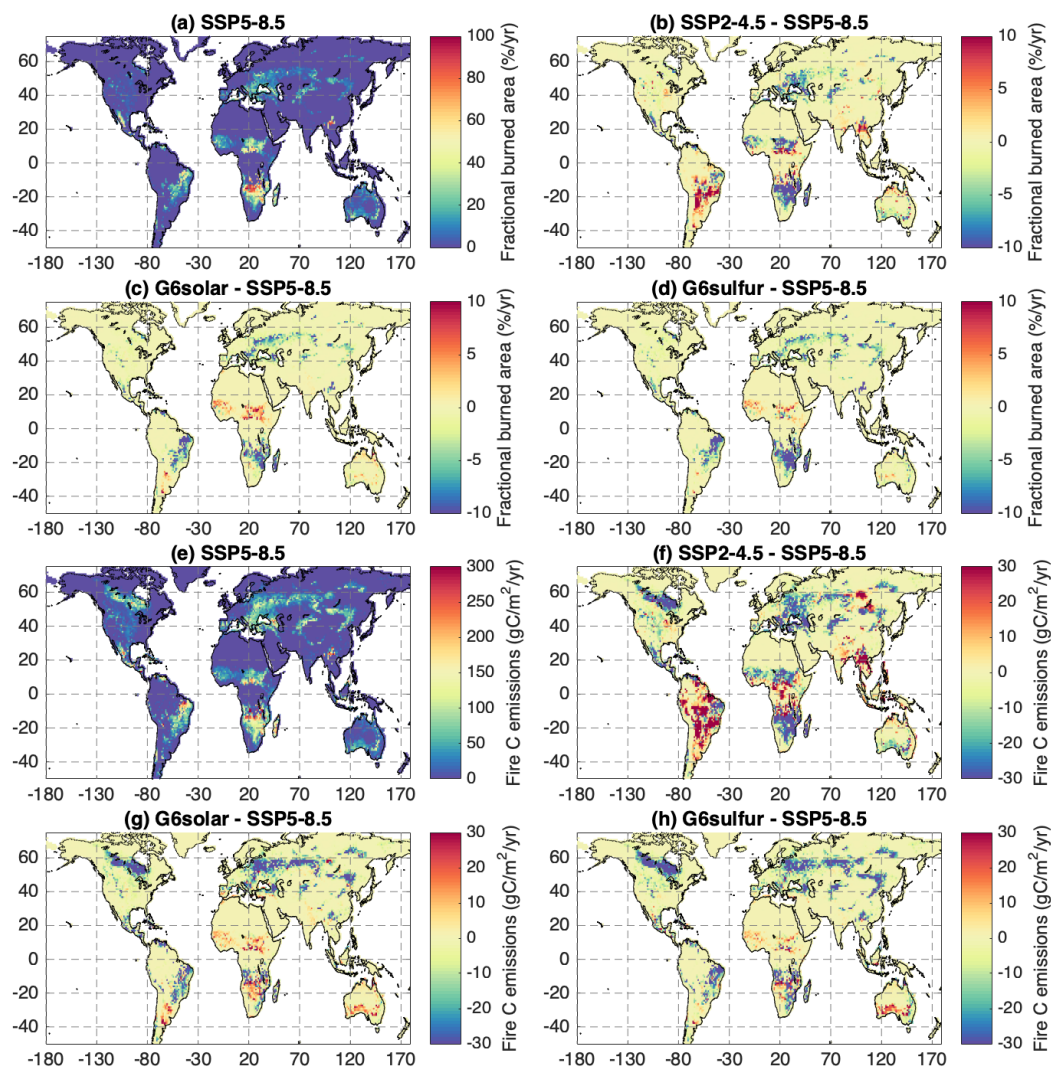


909
910
911
912
913
914
915
916
917
918
919
920
921
922

Figure 2. Overall global burned area and fire carbon emission trends and changes under the G6sulfur and G6solar geoengineering scenarios relative to SSP2-4.5 and SSP5-8.5. (a) Time series of global burned area from 2020 to 2100 under the G6sulfur, G6solar, SSP2-4.5, and SSP5-8.5 scenarios (represented by different colors). For the scenarios with multiple simulations, the ranges are also shown by the shaded areas. The time series are shown as 5-year moving averages. (b) Zonal changes (absolute value) of burned area in the period 2091-2100 relative to the period 2021-2030 (calculated by the value in 2091-2100 minus the value in 2021-2030), under the G6sulfur, G6solar, SSP2-4.5, and SSP5-8.5 scenarios (represented by different colors, color code is the same as it in panel a). 5-degree moving average were applied to the shown zonal changes. Panels (c) and (d) are similar to panels (a) and (b), respectively, but for fire carbon emissions.



923

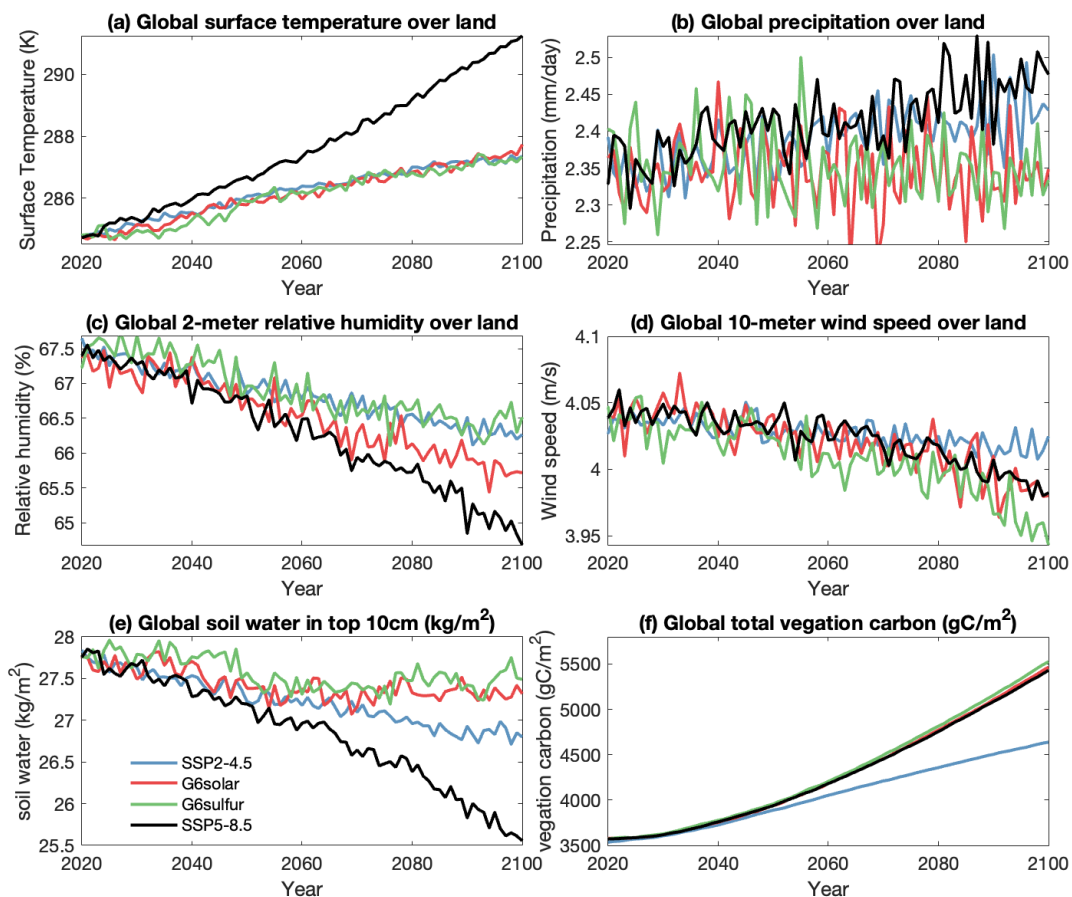


924
925
926
927
928
929
930
931
932
933

Figure 3. Fractional burned area (%/year) and fire carbon missions (gC/m²/year) averaged for 2091-2100. (a) Spatial distribution of fractional burned area (%/year) averaged for 2091-2100 under SSP5-8.5. The difference in surface temperature of (b) SSP2-4.5 from SSP5-8.5 (c) G6Solar from SSP5-8.5, and (d) G6Sulfur from SSP5-8.5 averaged for 2091-2100. (e-h) are similar to (a-d) but for fire carbon missions (gC/m²/year). For a scenario with multiple simulations (i.e., SSP5-8.5, SSP2-4.5, G6Sulfur, and G6Solar), simulation mean is shown.

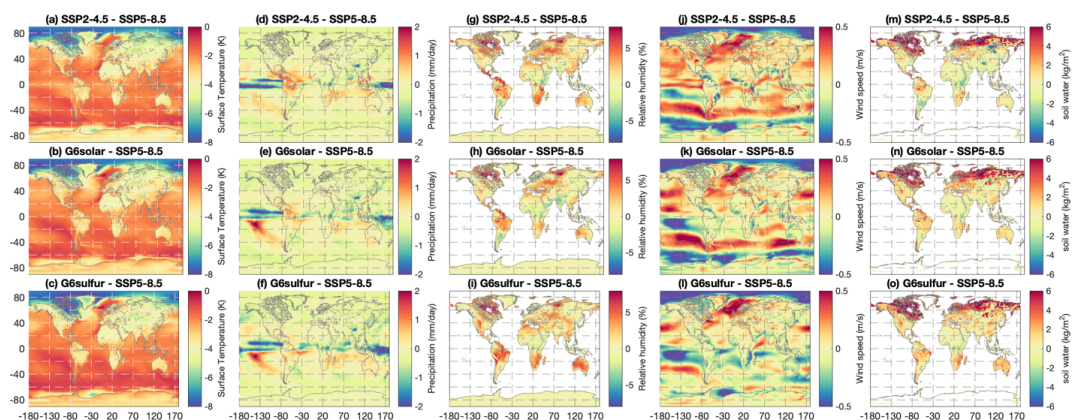


934
935



936
937
938
939
940
941
942
943
944

Figure 4. Time series of mean (a) surface temperature (K), (b) precipitation (mm/day) over the land, (c) 2-meter relative humidity (%) over the land, (d) 10-meter wind speed (m/s) over the land, (e) soil water content at top 10 cm (kg/m^2), and (f) vegetation carbon excluding carbon pool (Gc/m^2). For a scenario with multiple simulations (i.e., SSP5-8.5, SSP2-4.5, G6Sulfur, and G6Solar), simulation means are shown.

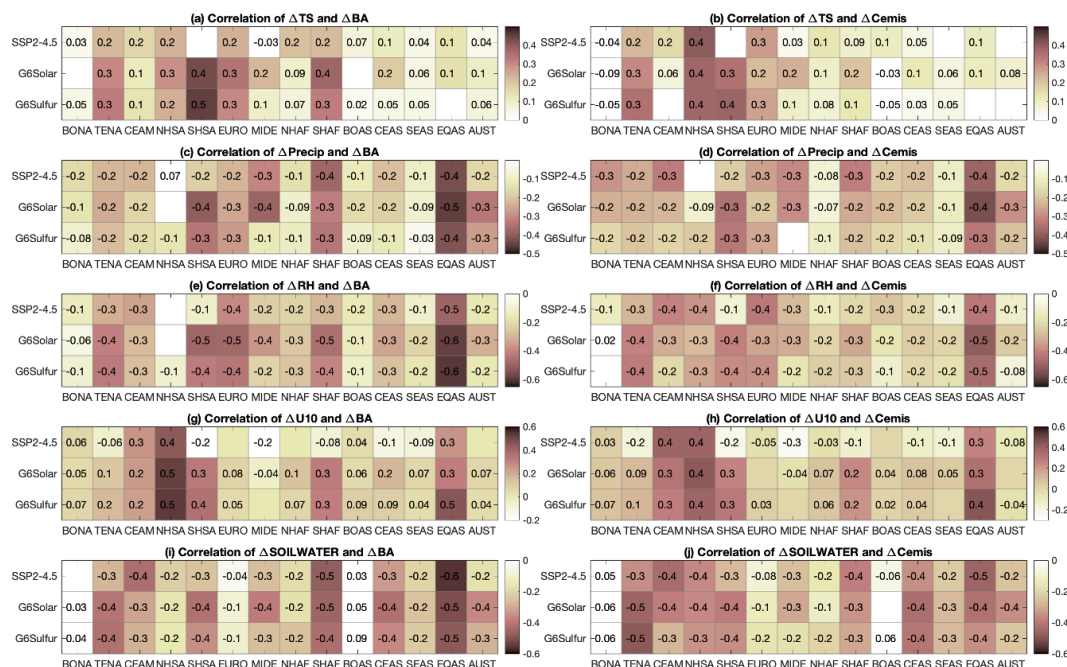


945
946
947
948
949
950
951
952
953
954
955

Figure 5. The difference in surface temperature (K) of (a) SSP2-4.5 from SSP5-8.5 (b) G6Solar from SSP5-8.5, (c) G6Sulfur from SSP5-8.5. (d-f) are the same as (a-c) but for precipitation (mm/day). (g-i) are the same as (a-c) but for 2-meter relative humidity (%). (j-l) are the same as (a-c) but for 10-meter wind speed (m/s). (m-o) are the same as (a-c) but for soil water content at top 10 cm (kg/m²).

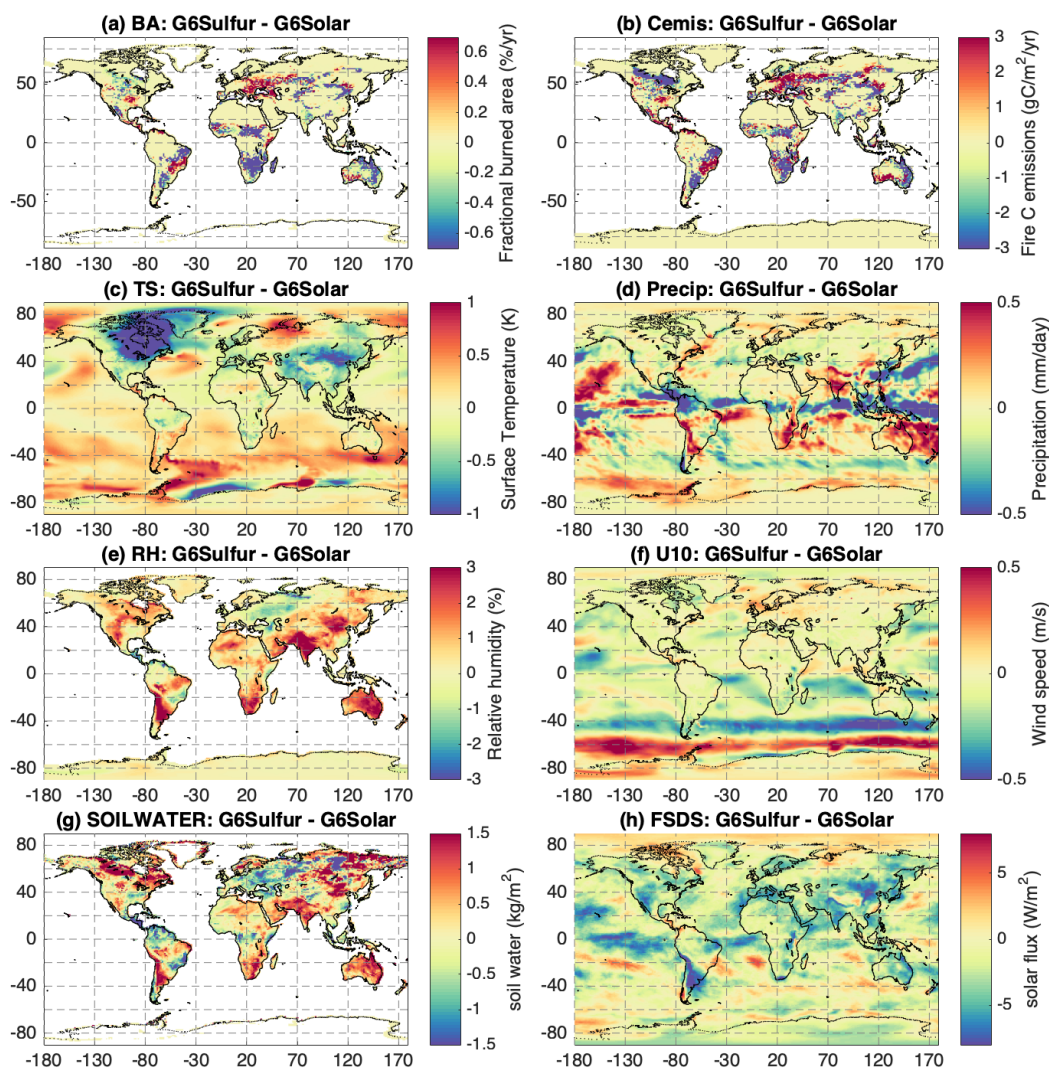


956



957
 958
 959
 960
 961
 962
 963
 964
 965
 966
 967
 968
 969
 970
 971
 972
 973
 974
 975
 976
 977
 978
 979

Figure 6. Correlations of (a) surface temperature change (ΔTS) and burned area change for SSP2-4.5, G6Solar, and G6Sulfur, and (b) ΔTS and fire carbon emission change ($\Delta Cemis$) for SSP2-4.5, G6Solar, and G6Sulfur. Only correlations that are significant are labeled (p value ≤ 0.1). For SSP2-4.5, ΔTS is calculated for individual model grids within the region and annual values. It is defined as TS of SSP2-4.5 minus TS of SSP5-8.5 (the reference case). For G6Solar and G6Sulfur, ΔTS is defined in the same way as SSP2-4.5. ΔBA and $\Delta Cemis$ are defined in the same way as ΔTS . (c-d) are the same as (a-b) but for precipitation change ($\Delta Precip$). (e-f) are the same as (a-b) but for relative humidity change (ΔRH). (g-h) are the same as (a-b) but for 10-meter wind speed change ($\Delta U10$). (i-j) are the same as (a-b) but for the change in soil water content at top 10 cm ($\Delta SOILWATER$). Correlations are calculated for 14 fire regions (x-axis), following Giglio et al. (2010), namely Boreal North America (BONA), Temperate North America (TENA), Central America (CEAM), Northern Hemisphere South America (NHSA), Southern Hemisphere South America (SHSA), Europe (EURO), Middle East (MIDE), Northern Hemisphere Africa (NHAF), Southern Hemisphere Africa (SHAF), Boreal Asia (BOAS), Central Asia (CEAS), Southeast Asia (SEAS), Equatorial Asia (EQAS), and Australia and New Zealand (AUST). The definition of the regions can be found in Figure S3.



980

981 **Figure 7.** The difference between G6Sulfur and G6Solar in (a) burned area fraction (BA; %/yr),
982 (b) fire carbon emissions (Cemis; gC/m²/yr), (c) surface temperature (TS; K), (d) precipitation
983 (Precip; mm/day), (e) 2-meter relative humidity (RH; %), (f) 10-meter wind speed (U10; m/s), (g)
984 soil water content at top 10 cm (Soilwater; kg/m²), and (h) downwelling solar flux at the surface
985 (FSDS; W/m²) averaged for 2091-2100.

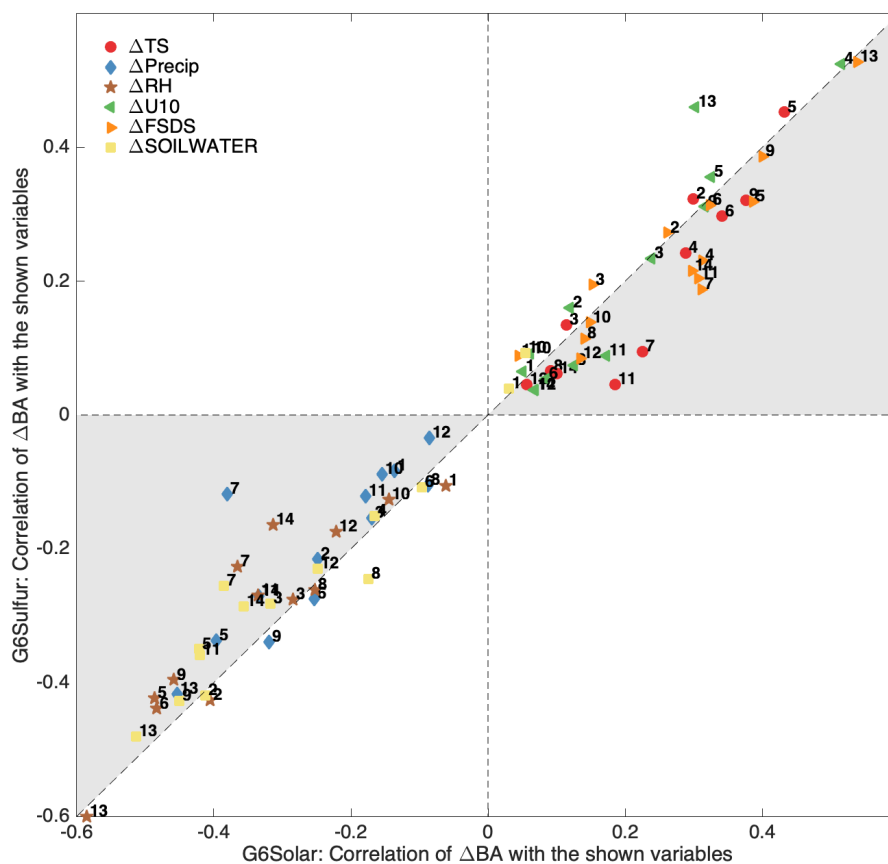
986

987

988

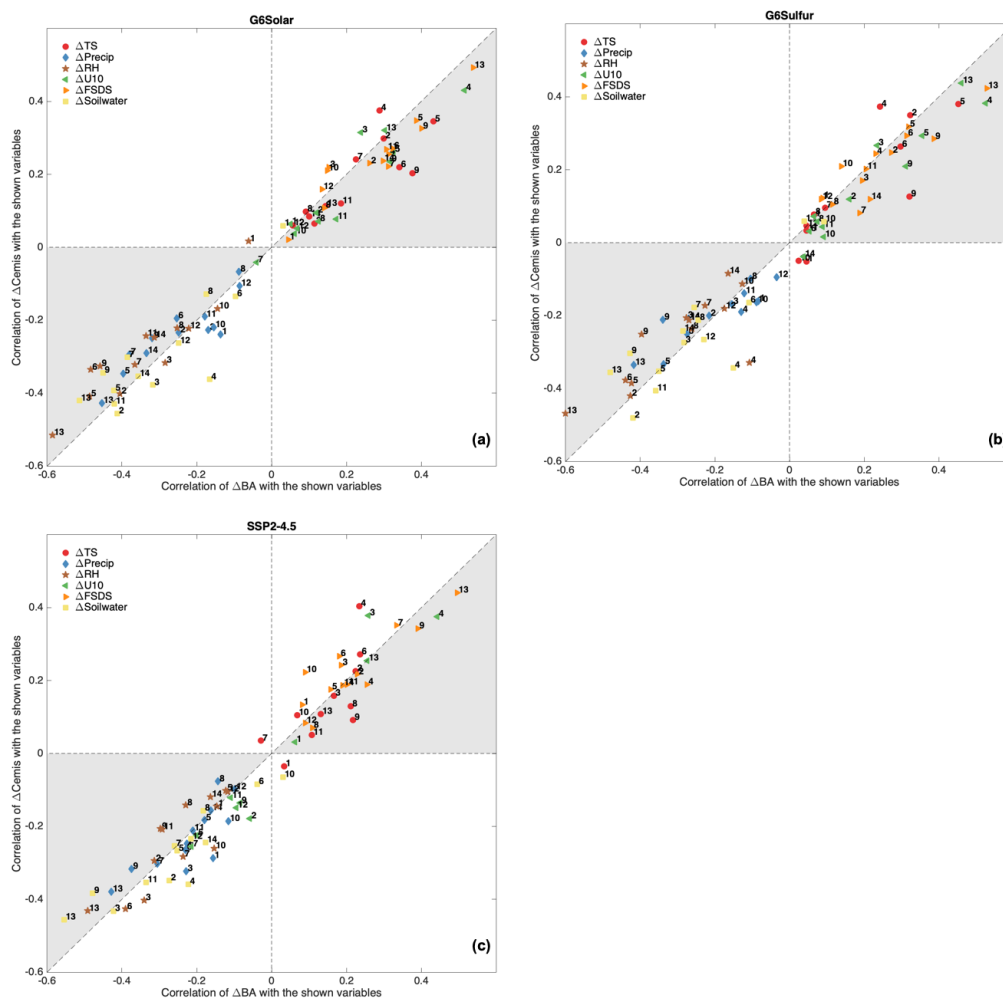
989

990



991

992 **Figure 8.** Correlations between burned area change in G6Solar from SSP5-8.5 (ΔBA) with the
993 change in other variables in G6Solar from SSP5-8.5 (x-axis) versus correlations between burned
994 area change in G6Solar from SSP5-8.5 (ΔBA) with the change in other variables in G6Sulfur from
995 SSP5-8.5 (y-axis). The variables shown here are surface temperature change (ΔTS), precipitation
996 change ($\Delta Precip$), 2-meter relative humidity change (ΔRH), 10-meter wind speed change ($\Delta U10$),
997 soil water content in top 10 cm change ($\Delta SOILWATER$), and downwelling solar flux at the surface
998 change ($\Delta FSDS$). The numbers labeled in the figure correspond to the region: 1–Boreal North
999 America, 2–Temperate North America, 3–Central America, 4–Northern Hemisphere South
1000 America, 5–Southern Hemisphere South America, 6–Europe, 7–Middle East, 8–Northern
1001 Hemisphere Africa, 9–Southern Hemisphere Africa, 10–Boreal Asia, 11–Central Asia, 12–
1002 Southeast Asia, 13–Equatorial Asia, and 14–Australia and New Zealand. The definition of the
1003 regions can be found in Figure S3. The shade highlights where correlation with ΔBA is larger than
1004 correlation with $\Delta Cemis$.



1005

1006 **Figure 9.** (a) Correlations between burned area change in G6Solar from SSP5-8.5 (Δ BA) with the
 1007 change in other variables in G6Solar from SSP5-8.5 (x-axis) versus correlations between fire
 1008 carbon emission change in G6Solar from SSP5-8.5 (Δ BA) with the change in other variables in
 1009 G6Solar from SSP5-8.5 (y-axis). The variables shown here are surface temperature change (Δ TS),
 1010 precipitation change (Δ Precip), 2-meter relative humidity change (Δ RH), 10-meter wind speed
 1011 change (Δ U10), soil water content in top 10 cm change (Δ SOILWATER), and downwelling solar
 1012 flux at the surface change (Δ FSDS). The numbers labeled in the figure correspond to the region:
 1013 1–Boreal North America, 2–Temperate North America, 3–Central America, 4–Northern
 1014 Hemisphere South America, 5–Southern Hemisphere South America, 6–Europe, 7–Middle East,
 1015 8–Northern Hemisphere Africa, 9–Southern Hemisphere Africa, 10–Boreal Asia, 11–Central Asia,
 1016 12–Southeast Asia, 13–Equatorial Asia, and 14–Australia and New Zealand. The definition of the
 1017 regions can be found in Figure S3. The shade highlights where correlation with Δ BA is larger than
 1018 correlation with Δ Cemis. (b) is the same as (a) but for G6Sulfur. (c) is the same as (a) but for SSP2-
 1019 4.5.